Reflector modelling of MTR cores making use of normalised generalised equivalence theory

Suzanne Anél Groenewald

Dissertation submitted in partial fulfilment of the requirements for the degree *Master of Science in Nuclear Engineering* at the Potchefstroom campus of the North-West University

Supervisor: F. Reitsma
Calvera Consultants
Roodepoort
South Africa

Promoter: Prof. E. J. Mulder
Department of Mechanical and Nuclear Engineering
North-West University
South Africa

December 2012

Acknowledgements

I give my sincerest gratitude to my husband Bernard, for his steadfast support and never-ending patience while I was working on this dissertation.

I would like to thank my supervisor, Frederik Reitsma. Thank you for your help, support and encouragement. My gratitude also goes out to Dr. Wessel Joubert, for his help with programming; to Rian Prinsloo, for always lending an ear when I needed to discuss anyting, and for encouragement; and to Dr. Francois Van Heerden, for building and running the Serpent model I used in this work.

Lastly I kindly thank Dr. Pavel Bokov, for all his technical comments, and Hantie Labuschagne, for editing and proof reading of my work.

Abstract

This research focuses on modelling reflectors in typical material testing reactors (MTRs). Reflectors present some challenges to the usual approach to full-core calculational models. Diffusion theory is standardly used in full-core calculations and is known to be inaccurate in regions where the flux is anisotropic, for example within the reflectors. Thus, special consideration should be given to reflector models. In this research, normalised generalised equivalence theory is used to homogenise cross-sections and calculate equivalent nodal parameters and albedo boundary conditions for the reflector surrounding a typical MTR reactor. Various studies have shown that equivalence theory can be used to accurately generate equivalent nodal parameters for the core and reflector regions of large reactors, such as pressurised and boiling water reactors, in one dimension and for two neutron energy groups. This has not been tested for smaller reactors where leakage, environment sensitivity and multi-group spectrum dependency are much larger.

The SAFARI-1 MTR reactor is modelled in this work. A thirty day operational cycle is simulated for this reactor, using the nodal diffusion code MGRAC. NGET reflector equivalent nodal parameters are calculated using the codes NEWT and EQUIVA. The impact of different reflector models are evaluated, based on their effect on the core power, flux distribution, reactivity and neutron leakage over the duration of the operational cycle.

It is found that homogenisation introduces some environment dependencies in the reflector parameters, particularly in the corners of the reactor core. In full-core calculations, the reflector parameters show some sensitivity to the in-core reflector structures, but not the fuel composition. A practical reflector model for SAFARI-1 is proposed, which proves that NGET equivalence theory can be used for multi-group reflector modelling in a small MTR reactor. This approach to reflector modelling simplifies the core model, increases the accuracy of a diffusion calculation, and increases the efficiency (shorter calculational time and better convergence behaviour) of computer simulations.

Keywords: reflector modelling, equivalence theory, homogenisation, equivalent nodal parameters, high leakage, environment sensitivity, multi-group.

Contents

List of Figures

List of Tables

Chapter 1

Introduction

To understand and predict the physical behaviour of a nuclear reactor core, the neutron distribution and interaction with matter must be known, at any given time, in any position in the reactor. From this, neutron reaction rates can be determined, which can be used to determine important design quantities such as power distribution, multiplication factors and reactivity coefficients.

The first chapter of this work outlines the need for accurate treatment of the reflector in a nuclear reactor. In Section 1.2 a short discussion is given on Material Testing Reactors, and why reflector modelling is particularly important in these types of nuclear reactors. The thesis objectives are discussed in Section 1.3 and Section 1.4 provides a layout of the rest of this work.

1.1 Overview

In order to describe the state that a nuclear reactor is in, the distribution of the neutron flux must be known. Once this is known, the reaction rates, reactivity coefficient, power distribution, etc. can be calculated. Thus the neutron distribution throughout the reactor must be determined. This distribution is described by the neutron transport equation. This equation is impossible to solve analytically for all but the most simplified and unrealistic reactor problems [1]. Therefore numerical methods are used to solve the transport equation. The deterministic approach to model a reactor starts by simplifying the transport equation enough to enable full-core calculations in reasonable time and accuracy.

To model a reactor, the geometry is divided into smaller areas called meshes or nodes, which, when coupled to each other, will represent the full core. Such nodes can be assembly sized (such as fuel assemblies, control assemblies, reflector and structural elements), multi-assembly or quarter assembly sized. The neutron transport equation is solved for these individual nodes, in two dimensions, with great geometric detail and a large number of energy groups (typically hundreds). These nodes can then be spatially homogenised so that the detailed geometric structure is lost and only an average representation of the node is conserved. Also, the detailed fine energy group structure can be condensed into a few broad energy groups (typically less than 10). A greatly simplified

version of the transport equation, for example the diffusion equation, can now be used to model the core in three dimensions, with simplified geometry and in few energy groups, by coupling the homogenised nodes through their interaction with one another.

The accuracy of the homogenisation technique will greatly influence the accuracy of the 3D model. Many studies have gone into improving the accuracy and the applicability of homogenisation techniques [2, 3, 4, 5].

Accurate representation of the reflector in a core model is very important. The reflector has a large influence on the core operation, since neutrons leaking from the core become thermalised in the reflector, and then get reflected back to the core, to induce further fission. Especially in smaller reactors, such as MTRs, where leakage is very high due to the small core dimensions, proper reflector modelling is essential. However, due to assumptions made in the derivation of the diffusion equation (anisotropic scattering and slowly varying flux gradients), reflector modelling presents its own set of challenges. The flux gradient at the core-reflector interface is very steep, thus the reflector surrounding a core has very anisotropic scattering. Accurate transport calculations and advanced homogenisation techniques are typically needed, in order to model reflector regions accurately.

Equivalence theory was developed about thirty years ago by Koebke [3] and Smith [5], to improve core neutronic homogenisation models for light water reactors. This homogenisation method has found wide-spread application in the nuclear industry. Previous work by Müller [6] and Reitsma [7] showed that normalised generalised equivalence theory can successfully be applied to PWR and BWR reflector modelling, in two neutron energy groups. This has not been tested for smaller reactors where leakage, environment sensitivity and multi-group spectrum dependency are much larger.

1.2 Material Testing Reactors and SAFARI-1

There are many different types of nuclear reactors. Reactors are divided into categories based on their function and makeup. For instance, Pressurised Water Reactors (PWRs), Boiling Water Reactors (BWRs) and High Temperature Reactors (HTRs) are all power reactors, used to generate electricity.

Another broad class of reactors is research reactors. Reactors in this catagory are very diverse in structure, which is determined by the reactor's function. For example, a reactor that functions as a neutron source for experiments, will be built to allow high neutron leakage from the core. On the other hand, if a reactor's purpose is to irradiate materials to create radioactive isotopes, then the core will be shielded and neutrons will be trapped in areas where irradiation is to take place.

Material Testing Reactors (MTRs) form a subcategory of research reactors. MTRs are used as a source of neutrons (and other particles) for use in experiments and the production of isotopes.

The SAFARI-1 reactor [8] is modelled in this work. It is a 20 MW tank-in-pool type MTR, owned

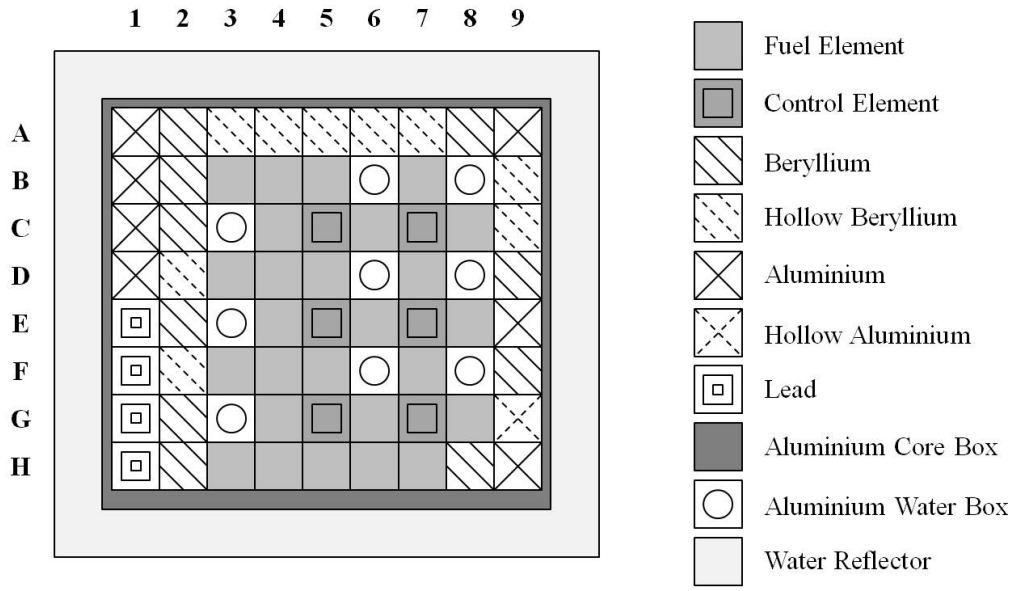

Figure 1.1: Schematic representation of the SAFARI-1 research reactor

and operated by Necsa at its Pelindaba site near Pretoria, South Africa. SAFARI-1 is an acronym for the South Africa Fundamental Atomic Research Installation.

An 8×9 grid houses 26 fuel elements, 5 control rods, 1 regulating rod, in-core irradiation facilities and reflector elements (see Figure 1.1). The size of the core is roughly $65 \times 65 \times 60$ cm, with a fuel pitch of 7.71×8.1 cm. The core is fuelled with flat-plate MTR type low enriched uranium fuel assemblies. The control assemblies consist of a cadmium neutron absorber element, with a fuel element attached below it. This type of control assembly is called a fuel-follower control rod. As the control rods are extracted from the core, the fuel followers get inserted into the core. These control rods are designed to extend the reactor operational cycle, by adding more fuel as the cycle progresses.

In-core reflectors include beryllium, aluminium and lead elements. The beryllium elements function as a neutron shield and surround the core on three sides. The pool-side of the core (so called because the core is exposed to the pool on this side) does not have beryllium reflectors. Neutrons leaking from the core at the pool-side, is used for silicon doping. The lead elements are used to shield the sensitive intrumentation just outside the core, next to the lead elements, from too high gamma radiation. The solid aluminium elements are simply filler elements, placed in the unused spaced in the core grid.

Some in-core reflector elements are hollow, with a water channel down the centre of the element. Small samples of various materials can be irradiated in these water channels. The in-core aluminium and water boxes act as thermal neutron traps, for the irradiation of materials. The core is surrounded by a thin aluminium core-box. The whole core is submerged into an open pool filled with light water, which functions as coolant, neutron moderator and reflector.

In summary, the SAFARI-1 core has a checkerboard configuration of fuel elements, control elements, and several different types of reflector elements. Such a heterogeneous core design is typical of MTRs, where functionality dictates the materials used in, and geometrical layout of the core.

1.3 Motivation and thesis objectives

The correct treatment of the reflector is important, since the reflector has a large influence on the neutron behaviour in and around the reactor core. The main objective of this work is to determine if normalised generalised equivalence theory (NGET) is a practical method for MTR reflector modelling. In order to be practical, reflector parameters should preferably be insensitive to changing core conditions, such as changing core-configuration, fuel burn-up, xenon build-up and control rod positions. Multi-group treatment is essential when modelling an MTR. MTRs are much smaller than power reactors and have a higher neutron leakage from the core. Two energy groups are not enough to capture this leakage spectrum accurately, thus 3 - 10 energy groups are typically used [9].

In this study, the accuracy of using NGET reflector parameters in full-core diffusion calculations is investigated. Errors introduced by homogenisation and size reduction of the reflector model is quantified. The environment dependence of the reflector equivalent nodal parameters is investigated, with emphasis on the fuel burn-up and the core environment adjacent to the reflector.

The efficiency of using NGET reflector parameters in full-core diffusion calculations is also discussed. Reflector size reduction and improved reflector modelling should reduce the computational time. This prediction is investigated.

The application of NGET theory to multi-group diffusion calculations is illustrated. In this work, full-core diffusion calculations are done in six broad energy groups.

This study will determine if normalised generalised equivalence theory is a practical method for MTR reflector modelling. The successful implementation will result in simplified core models, better accuracy and improved efficiency (shorter calculational time and better convergence behaviour) of computer simulations.

1.4 Thesis outline

This chapter briefly described the deterministic approach to full-core reactor modelling. In this approach the few-group diffusion equation is solved in a simplified core geometry obtained by assembly homogenisation. The accuracy of the homogenisation technique will greatly influence the accuracy of the full-core calculations. Accurate representation of the reflector in a core model is very important. High order transport calculations and advanced homogenisation techniques are typically needed, in order to model reflector regions accurately.

Equivalence theory has found wide-spread use as a method for reflector homogenisation. This method has successfully been used in PWR and BWR reflector homogenisation, but has not found widespread use in MTR modelling, for which accurate treatment of reflectors is essential. The main objective of this work is to determine if Normalised Generalised Equivalence Theory (NGET) is a practical method for MTR reflector modelling.

The calculational path used in the deterministic approach to reactor modelling is discussed in Chapter 2. Attention is given to nodal diffusion methods and homogenisation. Various methods used in reflector modelling is discussed, and Normalised Generalised Equivalence Theory (NGET) is derived. This homogenisation method is used for reflector modelling in this work.

Chapter 3 describes the computer codes and the models used in this work. The SCALE 6.1 and OSCAR-4 code systems are briefly described. Attention is given to the EQUIVA-1 code (part of the OSCAR-4 system). This code uses the NGET method to calculate equivalent nodal parameters for 1D reflector regions. A 1D verification model is defined, which is used to verify the calculational setup in this work. The SAFARI-1 reactor model is described, and is the main reactor model investigated in this work.

Verification and validation of the codes and calculational path is done in Chapter 4. The SCALE model is validated by code-to-code comparisons. The calculational path is verified by proving equivalence between the heterogeneous validation model, and the equivalent homogenised model. A discussion is given on the validation of the SAFARI-1 model in OSCAR-4.

Chapters 5 and 6 contain results for 1D reflector models and the SAFARI-1 model respectively. In Chapter 5, albedos and response matrices of various 1D reflector models are investigated. In Chapter 6, different reflector models for SAFARI-1 are defined and modelled. Conclusions are made as to which reflector models are suitable for use in SAFARI-1 support calculations.

Conclusions drawn from this work are presented in Chapter 7, and suggestions for future work are discussed.

Appendices A to E provide extra data and results for the 1D reflector and SAFARI-1 models.

Chapter 2

Theory

This chapter provides a general description of the calculational path used to model nuclear reactors in a deterministic approach. Neutron transport theory, diffusion theory and cross-section homogenisation are discussed in Section 2.1. Section 2.2 focuses on advanced homogenisation methods applied to reflector modelling.

2.1 Reactor modelling

This section provides a brief description of the calculational path that is generally used for reactor modelling, and also in this work. Lattice transport calculations, homogenisation and full-core diffusion calculations are discussed.

2.1.1 Transport approximation

The neutron transport equation is a linear form of the Boltzmann equation [10] describing diluted gas mixtures. Since no particle-particle interactions are taken into account, the equation becomes a linear first-order partial integro-differential equation, which is called the neutron transport equation [1]:

$$\begin{aligned} &\frac{1}{v}\frac{\partial \phi}{\partial t} + \hat{\Omega}\cdot\bar{\nabla}\phi + \Sigma_t \phi\left(\bar{r},\hat{\Omega},E,t\right) \\ &\qquad = \int_{4\pi} d\hat{\Omega}' \int_0^{\infty} dE' \Sigma_s\left(\hat{\Omega}'\rightarrow\hat{\Omega},E'\rightarrow E\right)\phi\left(\bar{r},\hat{\Omega}',E',t\right) + s\left(\bar{r},\hat{\Omega},E,t\right). \end{aligned} \tag{2.1}$$

In Equation (2.1), the dependent variable $\phi(\bar{r},\hat{\Omega},E,t)$ is the neutron flux, defined as $\phi(\bar{r},\hat{\Omega},E,t) = vN(\bar{r},\hat{\Omega},E,t)$ and measured in neutron/s/cm^2, where v is the neutron speed and $N(\bar{r},\hat{\Omega},E,t)$ is the neutron density. This variable depends on seven independent variables: neutron position ($\bar{r} = (x,y,z)$), direction in which the neutron is moving ($\hat{\Omega} = (\theta,\phi)$), neutron energy ($E$), and time at which the neutron is observed (t). The first term in the equation is the time rate of change of the neutron flux within a control volume. The second term describes the leakage into, and out of this volume (also called the streaming term). The third term describes the loss of neutrons from

the volume due to collisions and absorption. Σ_t is the total cross-section (sum of the scattering Σ_s and absorption Σ_a cross-sections) and is measured in cm^{-1}. The fourth term describes the gain of neutrons into the volume due to scattering from all other energies E' and angles $\hat{\Omega}'$. The fifth term is the neutron source term, describing the neutrons added to the volume by some neutron source $s(\bar{r}, E, \hat{\Omega}, t)$ [11].

This equation is complete with the definition of the initial conditions and boundary conditions. The initial conditions for this equation is simply $\phi(\bar{r}, \hat{\Omega}, E, 0) = \phi_0(\bar{r}, \hat{\Omega}, E) \,\forall\, \bar{r}, \hat{\Omega}, E$ for some initial neutron flux distribution. The boundary conditions depends on the specific problem and will not be further discussed here.

To summarise, the neutron transport equation is a balance equation that describes the neutron population in an arbitrary control volume. The rate of change of the neutron distribution in a volume is equal to the neutron gain in that volume (from sources, scattering and leakage into the volume) minus the neutron loss from that volume (due to scattering, absorption and leakage out of the volume).

In order to solve the transport equation numerically, some approximations have to be made. First, the seven independent variables have to be discretised. The time variable can be removed by considering only steady-state systems, such as criticality calculations. Later, when a solution to the transport equation is obtained, reactor dynamics can be investigated and time-dependence can be reintroduced. The energy range of interest in nuclear reactors typically range from 10 MeV to 0 eV. As an approximation, this energy range can be divided into smaller intervals, within which the neutron cross-sections are constant. In solving the transport equation, the energy range is typically divided into a few hundred discrete energy groups [12]. Cross-sections for these energy groups are calculated as follows:

$$\Sigma_{a,g} = \frac{\int_{E_g}^{E_{g-1}} dE\, \Sigma_a(E)\, \phi(E)}{\int_{E_g}^{E_{g-1}} dE\, \phi(E)}, \qquad \text{for } g = 1, 2, ..., G. \tag{2.2}$$

The spacial and angular dependencies must also be discretised before the transport equation can be solved. There are many ways to solve the transport equation, dealing with the spatial and angular dependencies in various ways. Examples of solution methods for the neutron transport equation is the Method of Characteristics [1], the P_N and S_N methods [12] and the Response Matrix Method [13].

Solving the transport equation for a large geometry, or in three dimensions, is still calculationally very expensive. Transport calculations are typically used to model small systems (or nodes) that represent parts of a reactor core, such as a fuel assembly, with a detailed representation in energy and 2D geometry. The steady-state multi-group transport equation is then solved for this system, using one of several solution methods (some are mentioned above). The solution to the transport equation yields the detailed flux distribution in the model.

2.1.2 Diffusion approximation

The 2D models (or nodes) calculated with the transport equation, is now homogenised. Homogenisation aims to represent a heterogeneous system with an approximate homogeneous system, in which the homogenised cross-sections are defined to preserve specific averages of the original heterogeneous system. Homogenisation is covered in Section 2.1.4.

A full-core model can be constructed for a reactor, consisting of a set of homogeneous nodes packed together to form the core. A simplified version of the transport equation can now be solved for the set of large homogeneous nodes, in 3D and in a few broad energy groups. Possible methods include diffusion theory [14], simplified P_N theory [1] and the response matrix method [13]. Diffusion theory is discussed here, since it is the method used in this work. Diffusion theory is derived from transport theory (2.1), where the following assumptions are made: isotropic sources and scattering, constant homogeneous parameters per spatial node, and an approximation relating the current to the flux [11]:

$$\bar{J}(\bar{r},t) = -D(\bar{r})\,\bar{\nabla}\phi(\bar{r},t), \tag{2.3}$$

$$D(\bar{r}) = \frac{1}{3\Sigma_{\mathrm{tr}}(\bar{r})} = \frac{1}{3(\Sigma_t - \bar{\mu}_0\Sigma_s)}. \tag{2.4}$$

Equation (2.3) describes the diffusion approximation, also known as Fick's law. It states that the neutron current $\bar{J}$ is proportional to the spatial gradient of the neutron flux ϕ. The proportionality coefficient is called the diffusion coefficient D. In Equation (2.4), Σ_{tr} is the transport cross-section and $\mu_0 = 2/3A$ is the average scattering angle cosine, where A is the atomic mass number of the scattering nuclei. With the above mentioned assumptions, the steady-state multi-group diffusion equation can be derived [1, 15], and is simply stated here:

$$-\bar{\nabla}\cdot D_g(\bar{r})\,\bar{\nabla}\tilde{\phi}_g(\bar{r}) + \tilde{\Sigma}_{r,g}(\bar{r})\,\tilde{\phi}_g(\bar{r}) = \sum_{g'\neq g}^{G}\tilde{\Sigma}_{s,g'\to g}(\bar{r})\,\tilde{\phi}_{g'}(\bar{r}) + \frac{\chi_g}{k_{\mathrm{eff}}}\sum_{g'=1}^{G}\nu_{g'}\tilde{\Sigma}_{f,g'}(\bar{r})\,\tilde{\phi}_{g'}(\bar{r}). \tag{2.5}$$

Here $\tilde{\phi}_g(\bar{r})$ is the homogenised flux in energy group $g \in G$. The first term of Equation (2.5) is the leakage term, describing the rate at which neutrons in energy group g leak out of the system. The second term is the removal term, where neutrons of energy group g gets removed via absorption and out-scattering. The removal cross-section for group g is defined as $\tilde{\Sigma}_{r,g} = \tilde{\Sigma}_{t,g} - \tilde{\Sigma}_{s,g\to g}$, i.e. the homogenised total scattering cross-section minus the self-scattering in group g. The third term is the collision source term, describing the rate at which neutrons scatter from all other energy groups g' into group g. The last term is the fission source term, describing the rate at which neutrons are created within energy group g via fission. Here $\nu_{g'}$ is the average number of neutrons released per fission reaction in group g' and χ_g is the fission spectrum for group g. $\tilde{\Sigma}_{f,g'}$ is the homogenised fission cross-section.

The factor k_{eff} is called the effective multiplication factor, and is defined as the ratio of the rate of neutron production by fission, to the rate of neutron loss by absorption and leakage. The k_{eff} is the fundamental eigenvalue for the steady state of the diffusion equation. Thus the diffusion equation

is also a neutron balance equation that sets the rate of neutron loss (leakage and out-scattering) equal to the rate of neutron gain (in-scattering and fission).

Equation (2.7) is solved for a reactor model, subject to the conditions that the neutron flux and the surface-normal component of the net current (i.e. the leakage) be continuous across all material interfaces in the model. Furthermore, appropriate boundary conditions are imposed on all external surfaces [16]. The reactor model is subdivided into nodes and each node have constant homogenised cross-sections and diffusion coefficients. The diffusion equation solves the node-averaged flux per node in the reactor. However, to solve this equation, additional equations are necessary, to couple the nodes in the system to each other, either by side-averaged flux or by currents [12].

2.1.3 Nodal diffusion methods

There are several ways to solve the diffusion equation (2.5), the most common ones being via finite difference methods [17], or one of several nodal methods [16, 15]. For nodal methods, the core is divided into relatively large nodes, the size of a fuel assembly in the radial plane, and axially divided so that the nodes are roughly cubical. Each of these nodes have a set of constant cross-sections and diffusion coefficients. In nodal methods, the diffusion equation (2.5) is integrated over the two directions transverse to each coordinate axis. Thus Equation (2.5) is integrated over the y and z-direction, to obtain a 1D equation that only depends on the x-direction, with two transverse leakage terms describing the flux interaction in the y and z-direction respectively. Similar equations are obtained for the remaining two directions [16].

The various nodal methods differ in how these 1D equations are solved. These methods can be broadly divided into two groups, namely polynomial methods and analytical methods. For polynomial methods, such as the Nodal Expansion Method (NEM) [18], the 1D fluxes are approximated by polynomials. There are many different types of polynomial methods, that differ in the choice of basis functions and expansion coefficients used for the polynomials. Analytical methods are based on the analytic solutions of the 1D transverse-integrated equations. Various methods exist to do this, such as the Analytical Nodal Method (ANM) [19] and the Nodal Green's Function Method [20]. In this work, the ANM method is used. In this method, an exact expression is obtained to couple the leakage from one node to the average flux in the two nearest neighbours. Furthermore, the transverse leakage terms are approximated by some or other shape, this being the only approximation introduced in the ANM formulation.

The solution to the nodal diffusion equation provides node-averaged flux and reaction rates, and face-averaged currents and fluxes for all the nodes, and the k_{eff} for the whole system. The node-averaged fluxes are normalised to the core power [5]. Although only nodal averages are calculated, detailed pin-power reconstruction (known as rehomogenisation) can be done in order to retrieve the heterogeneous flux in the fuel [21].

Due to the assumptions and approximations introduced by deriving the diffusion equation from the

transport equation, the diffusion equation (2.5) is only valid in media with a slowly varying current density in time, with anisotropic scattering and where the angular flux distribution is linearly anisotropic. Thus the diffusion equation becomes a poor approximation in regions near strongly absorbing media, localised sources and near boundaries with a big change in material properties. By treating detailed representative models accurately using transport calculations, and then homogenising these models to form large nodes with constant cross-sections and diffusion coefficients, it is possible to apply diffusion theory to most parts of a nuclear reactor. Where diffusion theory still falls short, correction factors are made, such as the introduction of discontinuity factors and the use of albedos, so that difficult areas do not have to be modelled explicitly.

2.1.4 Homogenisation theory

In order to represent the core with a collection of homogeneous nodes (to which the diffusion equation can be applied), the heterogeneous nodes have to be homogenised. Before diffusion theory can be applied, the core is discretised into spatial nodes and the cross-sections for each node is homogenised, or "smeared" over the node. Thus each node has a constant set of homogenised parameters, that preserves the heterogeneous transport solution in an average sense. For the homogenised node to be equivalent to the heterogeneous node (only in averages), the node-averaged reaction rate and the surface-averaged currents must be preserved. When this is preserved, the reactivity is automatically also preserved [5].

Consider the multi-group steady-state version of the transport equation [14]:

$$\bar{\nabla} \cdot \bar{J}_g(\bar{r}) + \Sigma_{t,g}(\bar{r})\,\phi_g(\bar{r}) = \frac{\chi_g}{k} \sum_{g'=1}^{G} \nu\Sigma_{f,g'}(\bar{r})\,\phi_{g'}(\bar{r}) + \sum_{g'=1}^{G} \Sigma_{g'\to g}(\bar{r})\,\phi_{g'}(\bar{r}). \tag{2.6}$$

A similar equation can be written for the homogenised model:

$$\bar{\nabla} \cdot \tilde{\bar{J}}_g(\bar{r}) + \tilde{\Sigma}_{t,g}(\bar{r})\,\tilde{\phi}_g(\bar{r}) = \frac{\chi_g}{k_{\text{eff}}} \sum_{g'=1}^{G} \nu\tilde{\Sigma}_{f,g'}(\bar{r})\,\tilde{\phi}_{g'}(\bar{r}) + \sum_{g'=1}^{G} \tilde{\Sigma}_{g'\to g}(\bar{r})\,\tilde{\phi}_{g'}(\bar{r}). \tag{2.7}$$

For Equation (2.7) to preserve the same average quantities calculated by Equation (2.6), the cross sections $\Sigma_{\alpha_i,g}$ per group g (where α represents the type of cross-section), must fulfill the following condition in any node i with volume V_i [5, 14]:

$$\int_{V_i} \tilde{\Sigma}_{\alpha,g}(\bar{r})\,\tilde{\phi}_g(\bar{r})\,d\bar{r} = \int_{V_i} \Sigma_{\alpha,g}(\bar{r})\,\phi_g(\bar{r})\,d\bar{r}. \tag{2.8}$$

Also, the side-averaged currents on all sides k of all nodes i must satisfy the equation:

$$\int_{S_{ik}} \tilde{\bar{J}}_g(\bar{r}) \cdot d\bar{S} = \int_{S_{ik}} \bar{J}_g(\bar{r}) \cdot d\bar{S}. \tag{2.9}$$

The homogenised parameters are assumed spatially constant in each node. If the diffusion Approximation (2.3) is used to simplify Equation (2.9), then Equations (2.8) and (2.9) lead to the following definitions for equivalent homogenised parameters:

$$\tilde{\Sigma}_{\alpha_i,g} \equiv \frac{\int_{V_i} \Sigma_{\alpha,g}(\bar{r})\,\phi_g(\bar{r})\,d\bar{r}}{\int_{V_i} \tilde{\phi}_g(\bar{r})\,d\bar{r}}, \tag{2.10}$$

$$\tilde{D}_{ik,g} \equiv \frac{-\int_{S_{ik}} \bar{J}_g(\bar{r}) \cdot d\bar{S}}{\int_{S_{ik}} \bar{\nabla}\tilde{\phi}_g(\bar{r}) \cdot d\bar{S}}. \tag{2.11}$$

In theory, the above criteria can be used to calculate diffusion parameters (flux-volume weighted cross-sections and diffusion coefficient) that will preserve the average properties of the heterogeneous node. However, inspection of Equations (2.10) and (2.11) reveal several practical difficulties. Firstly, the heterogeneous solution must be known before these equations can be solved. This defeats the whole purpose of homogenisation and the diffusion approximation, since these steps exist in order to solve a model that will be too time-consuming or difficult to solve with the transport equation. This issue is circumvented by solving the transport equation for some model that can represent the homogenised node, and using this model as reference for all similar homogenised nodes. Exact equivalence will not necessarily be met, since this heterogeneous model might not be identical to the true heterogeneous model, but this is usually a good approximation, that does not introduce large errors in the calculation. This calculation is referred to as an assembly heterogeneous calculation [5].

An example of this procedure is the modelling of a fuel assembly. Typically only one transport calculation is done, for an explicitly modelled fuel assembly (in 2D and with hundreds of energy groups) in an infinite fuel environment. This means that one fuel assembly is modelled, with reflective boundary conditions, using the transport equation. The set of homogenised cross-sections for this fuel assembly is then used for all the fuel assemblies in the core, even though not all the fuel elements are surrounded by fuel on all sides. The fact that different fuel assemblies are in different core environments (for example surrounded by fuel, or adjacent to a control element) is taken into account in the global core calculation, where these assemblies are modelled in their correct environment.

The second practical problem is that the homogeneous flux must be known before the homogeneous cross-sections can be calculated. But the homogeneous flux solution requires the homogenised cross-sections as input, therefore the above equations are non-linear. This issue is circumvented by also using the assembly heterogeneous calculation to represent the homogeneous flux [5]. In other words, for the assembly heterogeneous flux $\phi_{A,g}$, the homogeneous flux in Equation (2.10) is approximated as:

$$\int_{V_i} \tilde{\phi}_g(\bar{r})\,d\bar{r} = \int_{V_i} \phi_{A,g}(\bar{r})\,d\bar{r}. \tag{2.12}$$

The last impracticality is that if the conventional continuity condition of surface-averaged flux and currents are imposed on a node, the integrals in Equation (2.11) will in general be different for each surface k of the node. Thus it is not possible to define a constant value of the homogenised diffusion coefficient which preserves the surface-averaged currents over all the surfaces. Conventionally the diffusion coefficient is simply approximated as:

$$D_{i,g} \equiv \frac{-\int_{V_i} D_g(\bar{r})\,\phi_{A,g}(\bar{r})\,d\bar{r}}{\int_{V_i} \phi_{A,g}(\bar{r})\,d\bar{r}}. \tag{2.13}$$

However, this conventional approximation for the homogenised diffusion coefficient can introduce unacceptable large errors in the homogenisation procedure [5]. It was found that the homogenised diffusion equation, together with the continuity of the current and flux at node boundaries, does not have sufficient degrees of freedom, to preserve both surface currents and reaction rates [3].

In order to improve on this approach to homogenisation, advanced homogenisation methods are used. This work focuses on equivalence theory [2, 3, 5] homogenisation, described hereafter. For homogenised parameters to preserve both node-averaged reaction rates and surface-averaged currents of the heterogeneous model, the condition that the homogenised flux must be continuous at node interfaces, must be relaxed. A new continuity equation [5] is introduced:

$$\tilde{\phi}_i^+ f_i^+ = \tilde{\phi}_{i+1}^- f_{i+1}^- \tag{2.14}$$

at the node interface between node i and $i+1$. This interface condition allows for the homogeneous flux to be discontinuous across node boundaries, by the ratio of the discontinuity factors f_i^+ and f_{i+1}^- on the right hand side of node i and on the left hand side of node $i+1$, respectively. These discontinuity factors (DF) are defined as:

$$f_i^+ \equiv \frac{\phi_i^+}{\tilde{\phi}_i^+} \quad \text{and} \quad f_{i+1}^- \equiv \frac{\phi_{i+1}^-}{\tilde{\phi}_{i+1}^-} \tag{2.15}$$

and they add additional degrees of freedom to the homogenised nodal parameters. Equations (2.14) and (2.15) states that the heterogeneous flux at node boundaries must be continuous, but that the homogeneous flux is not. The homogeneous flux is discontinuous, by the ratio of the discontinuity factors on a node boundary. Whereas the heterogeneous flux must obviously be continuous, the homogeneous flux does not represent the real flux in the system, and therefore does not have to be continuous. Refer to Figure 2.1 for a graphical representation of the heterogeneous and homogeneous flux in two neighbouring nodes in a system.

This additional nodal parameter allows one to fix the diffusion coefficient to a unique value, thus circumventing the problem of a non-unique diffusion coefficient. The set of node-averaged cross-sections, diffusion coefficient and discontinuity factors per node, form the Equivalent Nodal Parameters (ENP) for that node. These ENPs are input to a diffusion solver. Equivalence theory

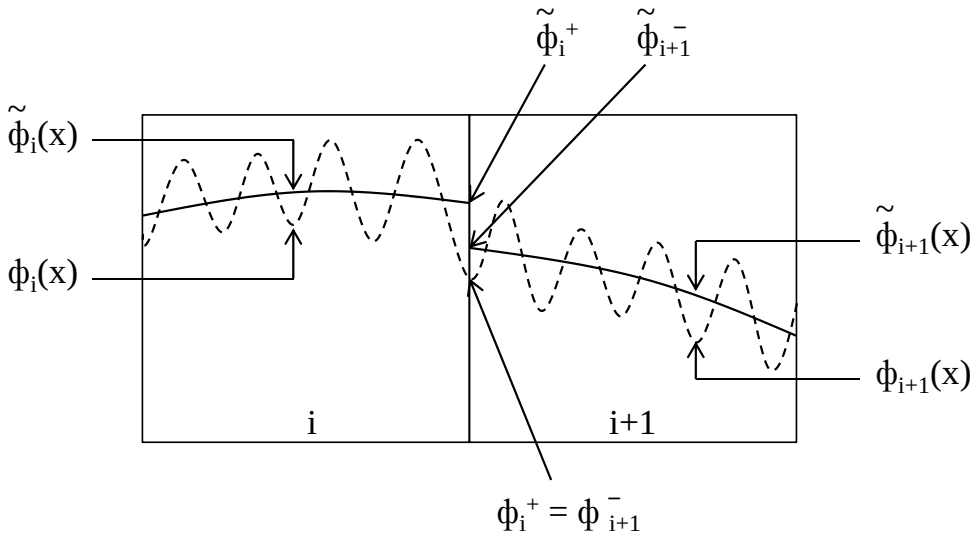

Figure 2.1: Heterogeneous and homogeneous flux across two nodes

reproduces the node-integrated properties: reaction rates and leakage rates, of the known reference heterogeneous solution.

Due to homogenisation, one can only calculate the global flux distribution. However, any local detailed flux distributions in fuel assemblies are lost. If some reference heterogeneous flux distribution is known, this flux distribution can be superimposed on the homogeneous flux distribution in a fuel assembly. In this manner, the heterogeneous flux detail can be recovered, and pin powers can be calculated for fuel assemblies. This process is known as rehomogenisation [21].

2.2 Reflector modelling

In Chapter 1, the importance of the reflector representation in core analysis was highlighted. The specific challenges in modelling small MTR reactors with high neutron leakage, were also discussed. In an MTR with many in-core and ex-core irradiation positions, where the flux levels should be known within a reasonable accuracy, the accurate representation of reflector regions becomes imperative.

Nodal diffusion methods are commonly used to perform full 3D core calculations. These methods were originally developed for the modelling of large commercial power reactors (PWR and BWR). The use of multi-group nodal solutions for MTR modelling have acquired acceptance in the 1990's [22]. The problem of modelling the reflector in the nodal approach, is to find a practical method to obtain few-group, homogenised nodal diffusion parameters to represent these regions in the model. Alternatively albedo boundary conditions can also be used. This chapter discusses homogenisation techniques which can be used in reflector modelling. Of these methods, the normalised generalised equivalence theory is discussed in detail, since this homogenisation method is used in this work.

2.2.1 Approaches to reflector modelling

A typical approach to full-core reactor calculations, is to solve the few-group diffusion equation in a simplified core geometry obtained by assembly homogenisation. Homogenisation is a technique to represent a heterogeneous model by a homogeneous model, that will preserve the average behaviour of the heterogeneous reference model. Homogenisation cannot preserve all the detail of a heterogeneous model. Only average parameters can be preserved. Homogenised components are constructed in such a way that the replacement of a heterogeneous component by a homogeneous one, will not change the global solution of the original heterogeneous system [23].

The flux in the reflector is often of no interest, and only the correct response that the reflector have on the core is important. For this reason, one of the oldest methods used to model the reflector around the core, is to replace the whole reflector by albedo boundary conditions at the core-reflector interface [24]. However, to achieve an accurate boundary condition, the calculation of the reference albedos has to be obtained from detailed 2D geometrical models, where the reflector explicitly is modelled, and a high-order transport calcualtion is utilised. The resulting albedos are strongly model-dependent [25]. Since such a detailed model is calculationally expensive to run, and the resulting albedos are only applicable to a certain core model, this approach for reflector modelling is not widely used in the industry.

If the albedo boundary condition is applied some distance away from the core, the environment-dependency of the albedo is drastically reduced. Thus representing the reflector by one reflector node and then an albedo, is a practical and feasible approach to reflector modelling.

Another approach to reflector modelling, is to represent the reflector structures around the core by an equivalent homogenised reflector, that can be used in full-core calculations. Just as assembly homogenisation is used to prepare broad-group homogenised cross-sections for fuel elements, reflector homogenisation is used in order to construct an equivalent reflector for use in the core calculations. However, since the reflector does not contain fissile material, a neutron source needs to be included in the reference model for reflector problems. Usually a simplified 1D core-reflector problem is used, for which parameters are calculated that will preserve the reflector's response on the core.

Several techniques exist to model the reflector region. Currently, the most widely used homogenisation method aims to preserve the heterogeneous flux boundary values, by using flux discontinuity factors (as discussed in Section 2.1.4).The original work on equivalence theory homogenisation was done by Koebke and Smith [2, 3, 4, 5]. Today, several adaptations of equivalence theory exist [26, 27, 28, 6, 29]. Other homogenisation methods include the use of current discontinuity factors, to preserve partial currents in the reference problem [30], 2D colourset calculations [31], or to represent the reflector by a response matrix [32, 6].

In this work, one such adaptation of equivalence theory is used for reflector modelling. This method, called Normalised Generalised Equivalence Theory (NGET) was developed for 1D multi-group reflector homogenisation and is discussed in the next section.

2.2.2 Normalised generalised equivalence theory

The homogenisation method described in Section 2.1.4 is known as Generalised Equivalence Theory (GET) [5]. The GET methodology leads to one more ENP than required, in order to define an equivalent homogenised problem. The face-dependant DFs are defined to preserve surface currents and therefore the diffusion coefficient (which is treated as an arbitrary parameter), is unnecessary in order to define the ENPs. In another equivalence theory based method, called Simplified Equivalence Theory [3], this fact is exploited, by using an arbitrary diffusion coefficient as a free parameter to define an equivalent homogenised problem. This method provides only one discontinuity factor per node, together with a diffusion coefficient. Thus SET uses exactly the necessary number of ENPs to define an equivalent homogenised problem [6]. Since there is only one DF per node, it is possible to divide all cross-sections and diffusion coefficients by the group DFs, obtaining equations that can be solved using diffusion codes which have conventional continuity conditions on interface fluxes [4, 5].

The disadvantage of SET is that the DF and diffusion coefficient is determined iteratively, which add unwanted calculational time. This method, as the name suggests, is an approximation, based on the assumption that the DF and the diffusion coefficient derived for one coordinate direction, are valid in all the directions of a node. It has been shown that this approximation is very accurate when modelling fuel in static PWR analysis [3, 26]. Furthermore, the cross-sections and diffusion coefficient is divided by the DF and used to define a new flux continuity condition $\tilde{\phi}_{i,g} = \phi_{i,g}^{\mathrm{SET}}/f_{i,g}$, the resultant flux per node is an unphysical quantity. Lastly, SET is limited to 2 energy group calculations only. For PWR and BWR reactors, this is not a limitation, as these reactors are typically modelled in 2 energy groups. MTRs though, are modelled with more energy groups, to capture the leakage spectrum more accurately.

The Normalised Generalised Equivalence Theory (NGET) is based on the principles of GET and SET theory. This method is only applicable to regions that can be presented by a single direction (axis), which is typically the case with reflector regions. This method is also not bound to a specific number of energy groups. NGET homogenisation theory [6, 33] is based on the observation that only the ratios of the discontinuity factors on a node interface are important in order to conserve the neutronic coupling between adjacent nodes in a system, and not the values themselves. Inspection of Equation (2.14), rewritten here with both discontinuity factors on one side of the equation, clearly shows that the ratio of two discontinuity factors on a node boundary provides the new flux continuity equation

$$\tilde{\phi}_i^+ \frac{f_i^+}{f_{i+1}^-} = \tilde{\phi}_{i+1}^-.$$

Using this observation, the NGET discontinuity factors are defined as:

$$\frac{F_{i,g}^+}{F_{i+1,g}^-} = \frac{f_{i,g}^+}{f_{i+1,g}^-}, \tag{2.16}$$

$$F_{i,g}^+ = F_{i,g}^- = F_{i,g}. \tag{2.17}$$

The first equation ensures the conservation of the original discontinuity factor ratios, while the second equation enforces that the new discontinuity factors are equal on both sides of a node i. By substituting the above definition for the NGET discontinuity factors ($F_{i,g}$) into Equation (2.14), the new, NGET flux continuity condition is obtained:

$$\tilde{\phi}^{+}_{i,g} F_{i,g} = \tilde{\phi}^{-}_{i+1,g} F_{i+1,g}. \tag{2.18}$$

This new criteria leads to $n-1$ parameters for n nodes. The n^{th} condition is obtained by setting one, lets say the left hand discontinuity factor of the first node, i_0, equal to the "old" discontinuity factor on that surface:

$$F^{+}_{i_0,g} = f^{+}_{i_0,g}. \tag{2.19}$$

Starting from this value, each consecutive discontinuity factor can be defined in terms of this first value. The discontinuity factors get normalised to this first value and thus the name of this method, Normalised Generalised Equivalence Theory (NGET).

The very last "old" discontinuity factor ($f^{+}_{N,g}$) remains unused at this stage. This DF is used to define the NGET albedo boundary condition at the end of the system in question. Adapting the GET albedo boundary condition to include the new DFs, the NGET albedo boundary condition is defined as:

$$\hat{\beta}^{+}_{N,gg'} = \frac{\frac{F^{+}_{N,g}}{f^{+}_{N,g}} \phi^{+}_{N,g} - 2J^{+}_{N,g}}{\frac{F^{+}_{N,g}}{f^{+}_{N,g}} \phi^{+}_{N,g} + 2J^{+}_{N,g}} \delta_{gg'}. \tag{2.20}$$

Here $\phi^{+}_{N,g}$ is the group g face-averaged flux on the outer surface of node N. Also, $J^{+}_{N,g}$ is the group g face-averaged, outward directed normal net current (i.e. face-averaged net leakage) for node N. This derivation is covered in detail in [6].

This single DF, together with flux volume weighted cross-sections and a diffusion coefficient form the ENPs for each node in a system. Since there is only one discontinuity factor per node (per energy group), this DF can be divided into the cross-sections for the node. Because it is divided into the cross-sections, no additional information is passed to the diffusion code and thus conventional diffusion theory codes can be used without any adaptations.

Note that this approach can only be followed in 1D models where only two node faces are defined. Furthermore, the NGET method was developed specifically for reflector homogenisation. Just like in the SET method, the discontinuity factors are divided into the flux for each node, resulting in an unphysical flux representation for that node. Usually only the response that the reflector have on the core is of interest, not the flux distribution in the reflector. This is not the case in the core itself, where the node-averaged flux distribution, as well as the reconstructed heterogeneous flux in each node is needed. Therefore the NGET method is only used to model reflector regions.

2.3 Summary

In the deterministic approach to reactor modelling, fine-group transport calculations are done for a number of reference problems. These reference results are used to generate a library of homogenised cross-sections. These homogenised parameters are used for broad-group core calculations. Homogenisation is necessary in order to replace heterogeneous components in a reactor, with homogeneous ones that will yield accurate average values in global diffusion calculations.

Accurate reflector modelling is very important, because the reflector plays an important part in core parameters such as leakage, reactivity and power distribution. Since the leakage is very high in an MTR, correct treatment of the reflector becomes even more important. Several techniques exist to model reflector regions. Normalised Generalised Equivalence Theory (NGET) is used for reflector modelling in this work.

Chapter 3

Codes and models

The first section in this chapter contains a description of the various codes used in this work. The second part describes the models that are calculated.

3.1 Description of codes

The calculational path is illustrated in Figure 3.1. Two transport codes are used in this work, namely NEWT (part of the SCALE system) and HEADE (part of the OSCAR system). These transport codes are used to generate cross-sections for very detailed 2D unit models of a reactor core (such as a fuel assembly). EQUIVA-1 is used to homogenise reflector cross-sections and generate NGET equivalent nodal parameters for reflector nodes. MGRAC (part of the OSCAR system) is used for full-core diffusion calculations, using parameters obtained with HEADE, SCALE and EQUIVA-1. These codes are discussed in more detail in the following sections.

3.1.1 SCALE 6.1

It is necessary to obtain a best estimate transport reference calculation in order to generate accurate ENPs for ex-core reflector regions. The leakage process in a reflector model must be represented as accurately as possible. The SCALE 6.1 code system [34] was selected for this. SCALE is used because it offers good accuracy, flexibility in geometry and high order scattering, all of which are necessary for modelling reflectors. In SCALE, the control module TRITON is used to set up models and to call NEWT [35], which calculates cross-sections for all the reflector models in this study. The NEWT code (part of the SCALE code system) is a discrete ordinates (S_N) code, here used in $S_{16}P_3$ mode. The standard 238-group SCALE cross section library based on the ENDF/B-VII data evaluation was selected for this work. Convergence criteria of 10^{-11} are used for the k_{eff}, inner and outer iteration and the thermal upscattering iterations. The 238 energy groups are collapsed to 6 broad energy groups; the energy-group boundaries are shown in Table 3.1. This group structure is used in all the codes described in this section.

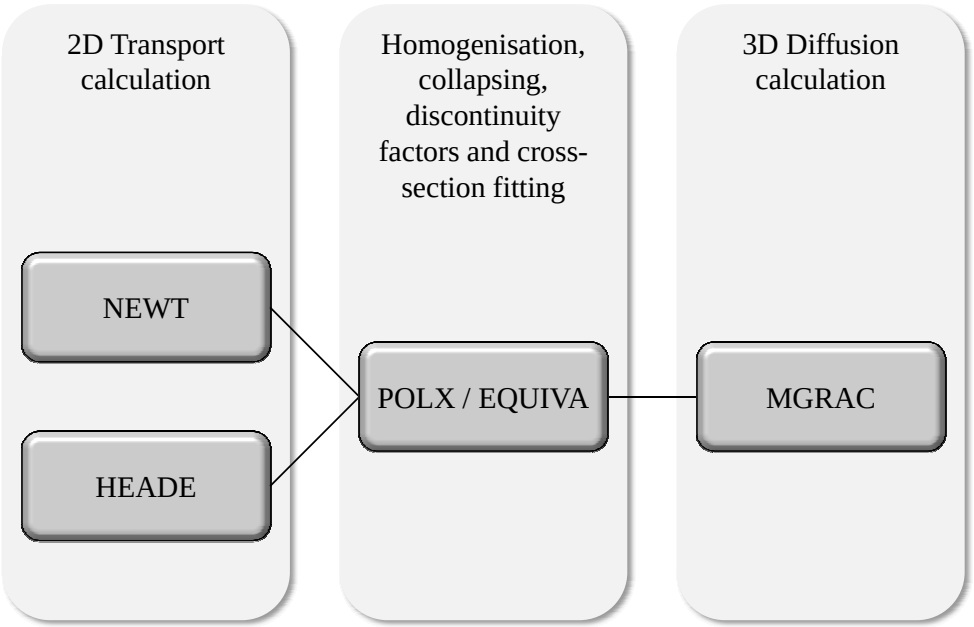

Figure 3.1: Flow diagram of the codes used in this work

Table 3.1: Broad-group energy boundaries

Group	Energy boundary (eV)
1	2.00×10^{7}
2	8.20×10^{5}
3	6.00×10^{3}
4	4.00×10^{0}
5	6.25×10^{-1}
6	1.50×10^{-1}

3.1.2 EQUIVA-1

EQUIVA-1 is an existing code in the OSCAR system and is used to generate ENPs for the reflector nodes, for 1D reflector representations. The EQUIVA-1 code [33, 36] uses NGET homogenisation to determine equivalent nodal parameters for reflector regions, from the results of one-dimensional (slab) multi-group transport calculations. This code has previously been used to generate ENPs for PWR [6] and BWR [7] reflectors. However, it has not been used for MTRs, which are very different to large power reactors in both the core-structure and reflector setup. In those studies, it was shown that the NGET reflector parameters show some sensitivity to the core environment, and that this environment sensitivity is introduced in the homogenisation of the reflector components. In an attemp to circumvent these homogenisation errors, EQUIVA-2 [6, 37] was developed. EQUIVA-2 combines the response matrices for different reflector regions, rather than to homogenise the regions into one bigger region.

This work only focuses on EQUIVA-1. The applicability of the NGET-RM method (EQUIVA-2) to MTR reflector modelling, can easily be investigated as future work, since no extra data is required to run EQUIVA-2 instead of EQUIVA-1.

A reference transport calculation must precede the EQUIVA-1 calculation. EQUIVA-1 requires face averaged boundary fluxes (heterogeneous) and net out-currents (or leakages), average fluxes, volumes, diffusion coefficients and cross-sections per material region as input. For this work, these parameters are obtained from the NEWT transport calculation. A conversion tool was developed, to read these parameters from the NEWT output, and write them in a form that EQUIVA-1 can read.

Figure 3.2 outlines the calculational procedure followed by EQUIVA-1. This code performs further group collapsing and homogenisation of reflector regions, if required. A two-point boundary value diffusion problem is then solved, for each node in the model, to obtain flux-volume weighted cross-sections for the reflector nodes. The analytic nodal diffusion method is used to solve the diffusion problem. The same nodal solution technique must be used in the calculation of the ENPs, as in the reactor calculations [3]. MGRAC (the diffusion solver in OSCAR-4) also uses the analytical nodal method. Should EQUIVA-1 be used with a different diffusion solver, then this method in EQUIVA will have to be changed to match the method used in the diffusion solver.

Standard GET discontinuity factors are then calculated for each node, and are used to calculate the NGET discontinuity factors. An NGET albedo boundary condition is calculated at the specified boundary (which does not have to be the last node boundary in the model) and lastly, the set of NGET equivalent nodal parameters are calculated. The NGET discontinuity factors are divided into the cross-sections and diffusion coefficient to form the NGET equivalent nodal parameters.

3.1.3 OSCAR-4

The OSCAR-4 code system [38, 39] is used in this study. OSCAR is a reactor analysis tool, developed and used by the South African Nuclear Energy Corporation (Necsa). The system consists

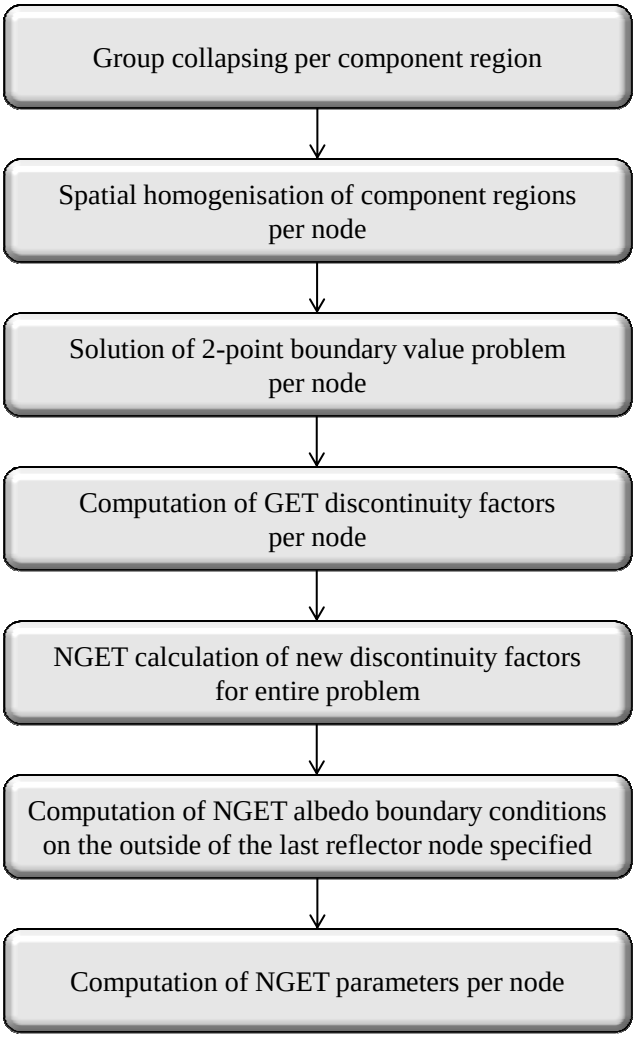

Figure 3.2: The calculational procedure in EQUIVA-1

mainly of a 2D lattice code HEADE (HEterogeneous Assembly DEpletion code), a 3D nodal core simulation code MGRAC (Multi-Group Reactor Analysis Code) and related service codes POLX and LINX.

HEADE [40] is a low order response matrix neutron transport code. A 172-group nuclear data library (based on JEFF 2.2) is used. HEADE produces a set of multi-group homogenised diffusion parameters for use in the global diffusion calculation. These parameters are fitted against state parameters (such as burn-up, fuel temperature, moderator density, etc.) in the POLX code. Cross-sections for all the core components are integrated into a single run-time cross-section library using the LINX tool. MGRAC is a three-dimensional multi-group time-independent diffusion solver, that uses the Multi-group Analytic Nodal Method (MANM) [41] to solve the one-dimensional transverse-integrated multi-group diffusion equations for a 3D model.

Cross-sections for all in-core materials are generated using HEADE. Only the ex-core reflector cross-sections are generated with SCALE and EQUIVA-1. All cross-sections are processed by POLX and LINX, to create one run-time cross-section library that is input to MGRAC. The parameters directly obtained from MGRAC, and used in this work, are: core reactivity (k_{eff}), assembly averaged flux and power distribution, and neutron leakage from the core.

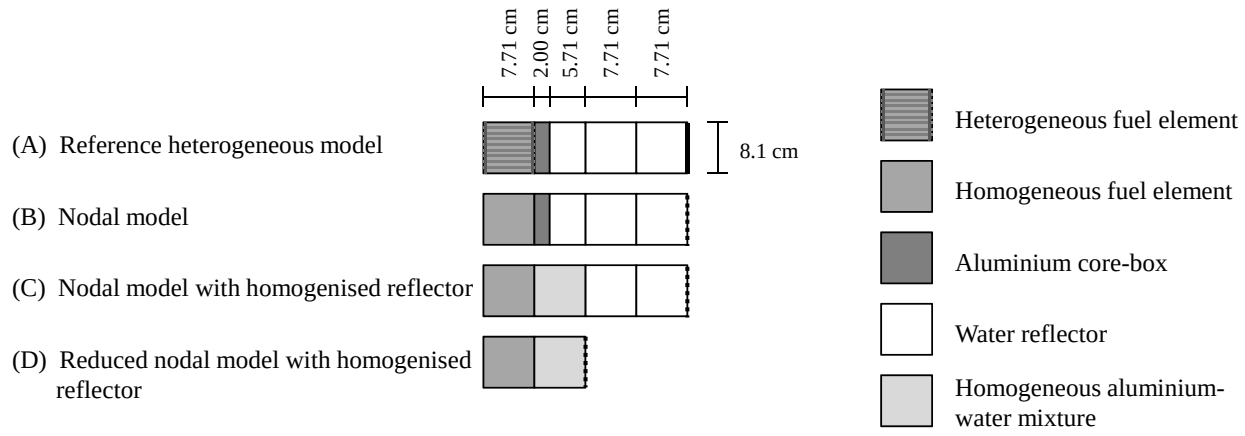

Figure 3.3: The one-dimensional verification model

3.2 Models defined

In this work, 1D reflector models, as well as 3D models of a nuclear reactor are used, and are described in this section. First, a model is defined for validation of the calculational path. Thereafter, the SAFARI-1 model is discussed.

3.2.1 Verification model

A simple fuel-reflector one-dimensional model (Figure 3.3) is used in order to test if the whole calculational path works. This model consists of a SAFARI-1 plate-type fresh fuel element (7.71×8.1 cm) as a fuel driver zone, an aluminium core-box (2×8.1 cm) and three water reflector nodes (5.71, 7.71 and 7.71×8.1 cm). These dimensions are the same as in the SAFARI-1 reactor, which is modelled hereafter.

The water reflector is about 20 cm thick and act as an infinite reflector in this setup. Studies carried out with SCALE indicate no change in reactivity when more water is added to this model, or when the boundary conditions at this distance from the core is changed. Previous work by Müller [42] indicates that the fuel thickness only need to be several neutron mfp long in order to simulate the spectral conditions in the reflector. The mean free path of neutrons in U-235 is roughly 2.7 cm and the fuel assembly is 7.71 cm thick. Therefore only one fuel assembly is used in the fuel driver zone for this model.

This model is set up in SCALE (model A in Figure 3.3) and the reference transport solution is calculated. SCALE performs homogenisation and group collapsing (from 238 to 6 energy groups), to produce cross-sections for the explicit nodal model (B in Figure 3.3) with a homogenised fuel assembly. These parameters are passed to EQUIVA-1, which calculates ENPs that is passed to MGRAC. Three separate sets of ENPs are prepared by EQUIVA-1. The first set is for the explicit nodal model (model B) and the second is for the nodal model with a homogenised box-water reflector node (model C). The last set of ENPs is for the reduced nodal model (model D), where the

first reflector node is the homogenised box-water node, and the rest of the reflector is represented by an albedo.

Model A have reflective boundary conditions on all sides, except after the outer water node, which have a vacuum boundary condition. Models B - D have an NGET albedo boundary condition on the outer node of the model. The rest of the model boundaries are reflective.

Cross-sections from models B to D are passed to MGRAC, where the diffusion equation is solved for these models. If the calculational path works as anticipated, then models A - D must have the same solution. Therefore this model serves as a verification for the calculational path.

3.2.2 SAFARI-1 model

The SAFARI-1 reactor [8] is modelled in this work. It is a 20 MW tank-in-pool type MTR. An 8×9 grid houses 26 fuel elements, 5 control rods, 1 regulating rod, in-core irradiation facilities and reflector elements (Figure 1.1). The core grid is 7.71×8.1 cm in the radial plane. Axially, the active core is almost 60 cm high.

In-core reflectors include beryllium, aluminium and lead elements. The core is surrounded by a thin aluminium core-box, and a light water reflector. At the pool-side of the core (row H in Figure 1.1), the fuel elements are adjacent to the core-box, with no in-core reflector between the fuel and the water.

An actual cycle in the operational history of the reactor (cycle C1001-1) is modelled in this work. This cycle was operational for 30 days, in January 2010. Two fresh fuel elements (positions B7 and H3) and two fresh control elements (positions C7 and G7) were loaded at the beginning of this cycle.

The core configuration of SAFARI-1 is very heterogeneous, and not all the parts of the reflector "see" the same core environment. Figure 3.4 illustrates the eight different core environments that the ex-core reflector in SAFARI-1 can see.

One of the objectives of this work, is to investigate the dependence of the reflector ENPs on the core environment. This study will determine whether all the reflector nodes can be modelled with the same set of cross-sections, or whether the reflector nodes need to be represented with unique cross-section sets, based on the core environment adjacent to the reflector nodes. Furthermore, the errors introduced by reflector homogenisation and the introduction of albedos are investigated. Lastly, the calculational time saved by modelling a smaller reflector, is discussed.

Several calculational models for SAFARI-1 are constructed in MGRAC. These models differ only in the way that the radial reflector is represented. In some models, the eight sets of ENPs are used, where in other models only one or two of the sets are used. The reflector is also modelled with an explicit reflector, an homogenised box-water reflector, and a reduced, homogenised reflector with albedo boundary conditions. Recall that Figure 3.3 illustrates the various treatments of the reflector models.

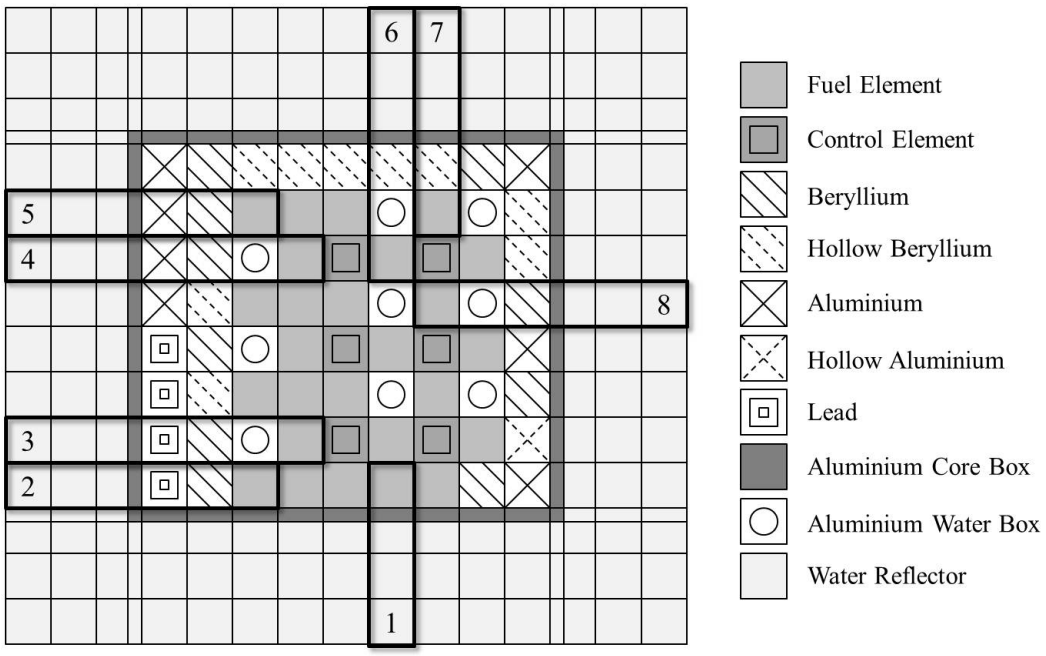

Figure 3.4: Schematic representation of the SAFARI-1 core, showing eight different 1D reflector cuts

3.2.3 1D cuts for SAFARI-1

Models are constructed in SCALE for these eight 1D planes or cuts (refer to Figure 3.5), and ENPs generated by EQUIVA-1. The dimensions used in the models are the same as that used in the SAFARI-1 model. The NGET parameters from these 1D cuts are used to represent the reflector nodes in full-core calculations with MGRAC.

The eight models are used to determine the impact of the in-core structure on the neutron spectrum in the reflector. To this end, albedo and response matrices are obtained for these eight 1D models. Results from SCALE and EQUIVA-1 are used for this part of the work. Thereafter, full-core calculations are done in MGRAC, using ENPs generated from these eight models.

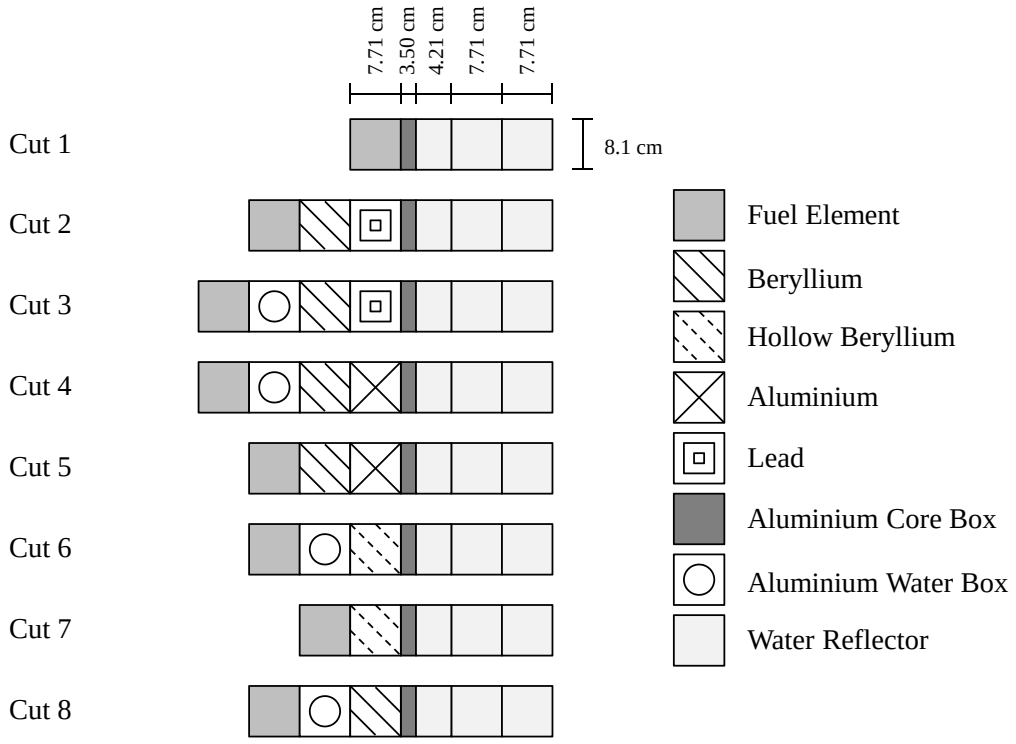

Figure 3.5: The eight 1D models representing the different reflector cuts in SAFARI-1

Chapter 4

Verification and validation

In this chapter the one-dimensional verification model showed in Figure (3.3) is used for verifying the equivalence between the reference transport solution and the diffusion solution. Some verification is also discussed for the SAFARI-1 model.

4.1 Verification of the calculational path

As a first step in setting up calculational models in this work, the calculational path is validated. Refer to Figure 3.1 for a description of the calculational path. As discussed earlier, the NGET homogenisation method should provide equivalence between the transport (SCALE, model A) and the diffusion (MGRAC, models B to D) problems. This section tests for equivalence between the transport and diffusion solutions.

4.1.1 SCALE and Serpent comparison

Studies have shown [43] that SCALE 6.1 (the latest version to date) can successfully be used as a lattice physics code. To test this, and to validate the model setup in SCALE, the same configuration (model A in Figure 3.3) is modelled in both SCALE and Serpent, but a reflective boundary condition was used on the outer boundary. The change in boundary condition was necessary due to limitations in the boundary condition treatment available in Serpent. Serpent [44] is a Monte Carlo continuous energy neutron transport code.

The 1D model is set up in both codes. The SCALE 238-group ENDF/B-VII library is used and results are collapsed to the six energy group structure given in Table 3.1. The continuous-energy ENDF/B-VII library is used in Serpent, and results are collapsed to the same six broad energy-groups as used in SCALE. Results are given in Appendix A and summarised here.

Reactivity and cross-sections are compared between the SCALE and Serpent models. The SCALE k_{eff} of 1.16248 is 287 pcm lower than the Serpent k_{eff}. The largest difference for the neutron flux is the group 6 thermal flux in the outer water node (water 3 in Table A.1). This value differs with

2.14 % between the two codes. The total cross-sections differ with about 4 % in group 6, in the water nodes (see Table A.2). The absorption cross-sections show excellent comparison, with the largest difference of 0.36 % in the fuel. The scatter cross-sections only show significant differences in the group 6 to 6 self-scatter cross-sections, with a difference of almost 5 % in the water nodes (see Tables A.1 to A.5). A difference of 1.39 % in the group 5 self-scatter cross-section for the aluminium core-box is also observed.

Results show that the two solutions are very similar and therefore give confidence in the use of SCALE as applied in this work.

4.1.2 EQUIVA-1 consistency check

The second part of the calculational path as seen in Figure 3.1, is the cross-section processing in EQUIVA-1 (refer also to Figure 3.2). The functionality of EQUIVA-1 has been tested extensively before [6, 45, 7], but is reconfirmed in this work.

The first of the three sets of cross-sections prepared by EQUIVA-1 (model B in Figure 3.3) is investigated here. This set is for the explicit nodal model, with no group collapsing and no homogenisation. For this model, EQUIVA-1 only calculates the discontinuity factors and albedo boundary condition. The discontinuity factors are then divided into the cross-sections. Thus, if the output cross-sections are multiplied with the discontinuity factors, they must be equal to the input cross-sections (obtained from the SCALE output). It was tested and verified: the exact input cross-sections are reproduced.

4.1.3 SCALE and MGRAC comparisons

EQUIVA-1 is used to compute ENPs for models B to D of the verification model (Figure 3.3). These models differ only in the reflector representation. Model B has an explicit reflector (small aluminium node and three water nodes), which is homogenised in model C (homogenised aluminium-water node and two water nodes). In model D, only the homogenised aluminium-water node is modelled. All three models have an NGET albedo boundary condition on the outer node of the model. For this verification test, the fuel cross-sections are also computed by EQUIVA-1, as a single assembly calculation [33]. Equivalent nodal parameters for all three models are passed to MGRAC, where these models are set up and a flux calculation is done for each of them. According to equivalence theory, results for all three these models should be the same as for the reference model in SCALE (model A in Figure 3.3).

This equivalence is confirmed. The k_{eff} for the heterogeneous transport model in SCALE is 1.16172. Exactly the same k_{eff} is calculated for all three models in MGRAC. Further inspection of the three models in MGRAC confirms that the three different reflector representations have exactly the same response on the “core” fuel element. Table 4.1 summarises the leakage from the “core”. These results are exactly the same for all three calculations.

Table 4.1: Leakage summary for the validation model

Description	Leakage (%)
Total	33.79
Axial	0.00
Radial	33.79
Radial epi-thermal	39.83
Radial thermal	-6.03

Table 4.2: Node-averaged flux per energy group for the explicit model B (neutron/s/cm^2)

Energy group	1 (Fuel)	2 (Core-box)	3 (Water)	4 (Water)	5 (Water)
1	2.47E+15	1.82E+15	9.79E+14	3.00E+14	8.53E+13
2	3.01E+15	2.10E+15	9.82E+14	1.81E+14	3.15E+13
3	2.19E+15	1.55E+15	8.24E+14	1.58E+14	2.70E+13
4	5.40E+14	3.90E+14	2.19E+14	4.03E+13	6.36E+12
5	5.35E+14	4.76E+14	3.94E+14	1.21E+14	1.76E+13
6	2.30E+15	3.39E+15	4.79E+15	1.91E+15	2.60E+14

Tables 4.2 to 4.4 show the node-averaged flux distribution per energy group for model B, C and D respectively. The power in the model is normalised to 0.69 MW, the power typically produced by one fuel element in SAFARI-1. The flux in the fuel is exactly the same in all three calculations. The flux in the reflector nodes differ for the various reflector models. Recall that this is not a physical flux quantity, because of NGET homogenisation. The flux in the homogenised reflector node for models C and D are the same, because this node is the same in both models. The albedo in model D preserves the same effect on the core as the two water nodes and the albedo combined in model C has.

As is evident from this section, the calculational path has been establised and equivalence was proven between a heterogeneous transport model and the homogenised nodal models (three different representations of the same system) with NGET parameters.

Table 4.3: Node-averaged flux per energy group for the explicit model C (neutron/s/cm^2)

Energy group	1 (Fuel)	2 (Reflector)	3 (Water)	4 (Water)
1	2.47E+15	1.25E+15	3.82E+14	1.08E+14
2	3.01E+15	1.46E+15	4.13E+14	7.20E+13
3	2.19E+15	1.21E+15	4.08E+14	7.00E+13
4	5.40E+14	3.15E+14	1.06E+14	1.68E+13
5	5.35E+14	4.44E+14	1.93E+14	2.80E+13
6	2.30E+15	3.63E+15	1.82E+15	2.49E+14

Table 4.4: Node-averaged flux per energy group for the explicit model D (neutron/s/cm^2)

Energy group	1 (Fuel)	2 (Reflector)
1	2.47E+15	1.25E+15
2	3.01E+15	1.46E+15
3	2.19E+15	1.21E+15
4	5.40E+14	3.15E+14
5	5.35E+14	4.44E+14
6	2.30E+15	3.63E+15

4.2 Validation of the OSCAR-4 SAFARI-1 model

The validation of the OSCAR code system and the associated SAFARI-1 model falls outside the scope of this work. The OSCAR calculational code system is used on a routine basis to perform core-follow calculations for the SAFARI-1 reactor [39]. The calculational path (HEADE to POLX to LINX to MGRAC) is thus extensively tested.

The SAFARI-1 model has been used to verify some of the MGRAC models [9, 46]. In [39] the first comparisons between a fully functional OSCAR-4, with many enhanced models, and OSCAR-3 were made. This work focused on the relative improvements in the code models, and also on comparisons to plant data from SAFARI-1. The control rod reactivity curves (S-curves) showed a marked improvement compared to the OSCAR-3 results, where the control rod movement and the fuel follower was modelled in an approximate way.

Work on the OSCAR-4 SAFARI-1 model validation is still in progress, and the new reflector models proposed in this work will be included in this validation effort.

OSCAR-4 is also being used in the Coordinated Research Project (CRP) of the IAEA, to validate calculational methods applied to research reactors. In this effort, several test problems are being evaluated and compared to plant measurements. The OPAL reactor in Australia [47], the MNR reactor in Canada [48] and the ET-RR2 reactor in Egypt [49] are amongst these. The final Tecdoc report is expected in 2013.

Chapter 5

Results: 1D cuts for SAFARI-1

The main objective of this chapter, is to investigate the dependence of the reflector ENPs on the core environment, in one dimension only. The eight 1D models in Figure 3.5 are investigated. Models are constructed in SCALE for these eight cuts. From the SCALE results, the fine group albedo at various node interfaces are obtained and discussed in the next section. Parameters are passed to EQUIVA-1, which calculates among other things, the reflection and transmission response matrices for a model. These matrices are investigated in the second section. Some concluding remarks are given in the last section of this chapter.

5.1 Fine group albedo

It is known that the use of albedo boundary conditions to represent the reflector, is not practical (see Section 2.2.1). This is mainly due to the environment dependence of the reflector on the core configuration, and the need for expensive and detailed reference 2D models to obtain accurate albedos. The inclusion of the fine-group albedo results calculated for the different 1D cuts are therefore not an attempt to apply them to the core models, but rather to investigate how the reflector response differs due to the fine-group spectrum differences in the various models.

From the SCALE printout, the 238-group flux and leakage are obtained, on each surface of the reflector nodes (i.e. on the core-reflector interface, on the outer boundary of the core-box, on the outer boundary of the first, second and third water nodes). From these values, the albedo is calculated, for all eight cuts, at all node boundaries in the reflector. The albedo is defined as:

$$\vec{j}_i^{\text{in}} = \hat{\beta}_i^{+}\, \vec{j}_i^{\text{out}},$$

where $\hat{\beta}_i^{+}$ is the albedo column vector (for the number of energy groups) on the outer surface of node i and $\vec{j}_i^{\text{in/out}}$ is the inward/outward directed partial current on the outer surface of the node. The partial currents are defined using the standard expression for diffusion theory [6]:

$$\vec{j}_i^{\text{in}} = \frac{1}{4}\bar{\phi}_i^{+} - \frac{1}{2}\bar{J}_i^{+},$$

$$\bar{J}_i^{\text{out}} = \frac{1}{4}\bar{\phi}_i^+ + \frac{1}{2}\bar{J}_i^+.$$

Here $\bar{\phi}_i^+$ is a column vector of the face-averaged flux on the outer surface of node i and $\bar{J}_i^+$ is the column vector of the face-averaged outward directed normal net current (i.e. net leakage) on the outer surface of node i. Thus the diagonal albedo matrix on the outer surface of node i can be defined as:

$$\hat{\beta}_{i,gg'}^+ = \frac{\phi_{i,g}^+ - 2J_{i,g}^+}{\phi_{i,g}^+ - 2J_{i,g}^+}\,\delta_{gg'} \tag{5.1}$$

for all $g, g' \in G$, where G is the number of energy groups.

The albedo values at various node-interfaces are calculated from the SCALE results. In Appendix B, plots are given for the albedo values for the different 1D cuts (see Figure 3.5).

The albedo on the core-reflector interface (thus the inner boundary of the core-box) for the eight different cuts, and defined in the 238-group structure used in the SCALE calculation, are shown in Figure B.1. The albedo at the core-reflector interface varies considerably between the different reflector cuts, even though they all represent the response of the core-box and water reflector. For instance, the reflector models with more aluminium (Cuts 4 and 5) shows a larger albedo value at very low energies. The reflector cuts with lead assemblies (Cuts 2 and 3) have a visible increase in the albedo at 0.0277 eV. These effects are all caused by the variation in the fine group currents at these energies.

In an effort to try and decrease the environment effects of the core on the reflector, it is customary to define the core model boundary condition or reflector cut-off so that at least one reflector node is still explicitly modelled around the core. In commercial LWRs this reflector node is typically the same size as the fuel assemblies. Using the same approach here for MTR applications, with much smaller node sizes, means that the node is only about a third of the selected reflector's size.

The albedo after this reflector node (beyond the corebox and first water node) shows much less environment sensitivity, as can be seen in Figure B.2. Still some differences in the albedo remains. For this albedo an absolute difference of 20 % is seen between the maximum and minimum values at any given energy. If Cut 1 (which is an outlier compared to the rest, since the fuel lies next to the water reflector) is excluded from this comparison, the differences are reduced to less than 9 %. Note that the shape of the albedos in Figure B.2 is much more consistent for all the cuts. It is clear that the nearly 6 cm of water included in the model, has already reduced the spectrum differences to a very large extend.

The comparison of the albedos on the core-reflector interface for Cut 1 with a fresh fuel and burnt fuel driver zone is shown in Figure B.3. This comparison shows an interesting result in the sensitivity to fuel burnup. The behaviour of these albedos is very similar but clearly shows some of the neutron spectrum differences between fresh and burned fuel. The presence of fission products in the burnt fuel makes the leakage spectrum from the fuel harder, as thermal neutrons are absorbed in the fission products, most notably Xenon-135. A small amount of plutonium is also present in the burnt fuel and some of the effects of the lower lying resonances of Pu-239 have a small impact

Table 5.1: Reflection and transmission matrices for Cut 1

To/From	1	2	3	4	5	6
1	0.11	0.00	0.00	0.00	0.00	0.00
2	0.18	0.15	0.00	0.00	0.00	0.00
3	0.06	0.18	0.04	0.00	0.00	0.00
4	0.01	0.03	0.10	-0.23	0.00	0.00
5	0.01	0.02	0.06	0.17	-0.26	0.04
6	0.02	0.07	0.19	0.44	0.68	0.44

To/From	1	2	3	4	5	6
1	0.37	0.00	0.00	0.00	0.00	0.00
2	0.15	0.28	0.00	0.00	0.00	0.00
3	0.05	0.14	0.25	0.00	0.00	0.00
4	0.01	0.03	0.06	0.07	0.00	0.00
5	0.01	0.02	0.04	0.06	0.05	0.02
6	0.02	0.06	0.17	0.32	0.34	0.30

on the leakage spectrum and the albedo. These differences are only noticeable at the core-reflector interface. The albedo after the first water node is practically identical for fresh fuel and burnt fuel models.

5.2 Broad group response matrix

Cross-sections for the eight 1D cuts are passed to, and processed by EQUIVA-1. The core-box and first reflector node are homogenised, NGET parameters are calculated for the reflector nodes, and the NGET albedo (see Equation (2.20)) is calculated on the outer surface of the first reflector node (which is now a homogenised mixture of the aluminium and water). The albedo response matrix and transmission response matrix for this reflector node are also calculated. For a derivation of these matrices, and an explanation of how EQUIVA-1 calculates them, refer to [6].

A reflection matrix for a node provides the probabilities that neutrons incident on that node, will be reflected back out of the node. Similarly, a transmission response matrix for a node provides the probabilities that neutrons incident on that node, will be transmitted through that node. Both of these are $g \times g$ matrices (for g energy groups).

The reflection and transmission matrices for Cut 1 (refer to Figure 3.5) are given in Table 5.1. Several conclusions can be drawn from these matrices. The highest values in the reflection matrix are in the thermal energy groups. The fast groups have much smaller fractions, as expected. Evidently, the thermal albedo is large, since neutrons are thermalised in the reflector and then reflected back to the core. Very few neutrons with such high energies get reflected back to the core.

The fact that the transmission matrix values are comparable to the reflection matrix values, confirms that one reflector node is not enough to capture all the neutrons leaking from the core (in this work, three assembly-sized reflector nodes were used). A large percentage of neutrons are transmitted through the first reflector node. Therefore it is very important that the albedo placed after the first water node, correctly preserves the response of the rest of the reflector on the core.

The response matrices for the other seven cuts are given in Appendix C. Comparing Cut 2 with Cut 1 shows that the thermal reflection of neutrons is much less in Cut 2 than in Cut 1. This cut have a beryllium and lead in-core structure, whereas in Cut 1 the fuel is adjacent to the reflector. These in-core structures cause a spectrum shift in the neutron leakage. Because of the group collapsing, this spectrum shift is visible in the response matrix of the reflector.

Closer inspection of response matrices for Cuts 2 to 8 (Tables C.1 to C.7) reveals that the response matrices for these models are very similar in value. They all differ from the response matrices for Cut 1. Cut 1 is the only model where the fuel is directly adjacent to the reflector. The other models have in-core structures (beryllium, lead, aluminium, water) between the fuel and the ex-core reflector. The response matrices in the reflector, for these models, are expected to be similar.

5.3 Summary of results

Albedo values at the core-reflector interface show sensitivity to the in-core structures (refered to as the core environment). The largest differenes in albedos for the eight 1D cuts are seen in the thermal energy range. The albedo show much less sensitivity to the core environment, when it is placed not at the core boundary, but after the first reflector node. By moving the model cut-off so that one reflector node is included in the core-reflector model, the sensitivity of the environment sensitivity of the albedo boundary condition is reduced drastically.

The leakage spectrum in the reflector is dependent on the core environment. The response matrices for the reflector in the the eight different 1D cuts differ from each other. These differences are introduced when the 238-group results are collapsed to 6 energy groups. The Cut 1 response matrix can differ with up to 9 % from the rest of the response matrices (with the largest differences in the thermal groups). The rest of the cuts have similar reponse matrices. Cut 1 is the only model where the fuel is directly adjacent to the reflector. The other models have in-core structures (beryllium, lead, aluminium, water) between the fuel and the ex-core reflector.

The dependencies of the reflector reponse to the core environment observed in this chapter, is only on a local scale. Considering that the leakage from the core happens mainly in the fast energy groups, and that environment dependencies observed here is mainly in the thermal groups, the importance of these dependencies can only be determined in full-core calculations, where their global impact can be established. This is done in the next chapter.

Chapter 6

Results: SAFARI-1 model

This chapter contains results for SAFARI-1 full-core calculations. The first part of this chapter provides results of the reference calculation. The effects of reflector homogenisation and size reduction are discussed in Sections 6.2 and 6.3. The dependencies of the reflector ENPs on the fuel driver zone and the core environment are covered in Sections 6.4 and 6.5. The last section of this chapter summarises the findings of the full-core calculations.

6.1 Reference model

In this section, the reference calculation is defined and results for this calculation are discussed. For the reference model, the ex-core reflector regions are modelled explicitly. Therefore the core-box is defined as a separate material region (or mesh), followed by the outside water regions. NGET parameters calculated by EQUIVA-1 are prepared for each separate region, thus no homogenisation is done. The eight 1D reflector cuts identified before, are used to represent all the different reflector regions. The geometrical layout of the reference model can be seen in Figure 6.1, with the numbers on the outer mesh corresponding to the numbers of the 1D reflector cuts applied to these regions. Figures 3.4 and 3.5 provide more information on the eight 1D cuts.

No special models were prepared for the ex-core corner nodes. The most appropriate cross-section set or material was selected and assigned to each node. This approximation is seen as sufficiently accurate, since these outer reflector corner nodes are of less importance, as they only share a corner with the corner node of the core, and not a full face (not a direct neighbour).

This SAFARI-1 core model is constructed to be a reference diffusion solution. Since the core-box is treated explicitly, no errors in reflector parameters due to homogenisation is introduced. Furthermore, the NGET parameters used to represent the different reflector regions are all exact in 1D, and are generated with the most appropriate environment. The group condensation errors should therefore also be limited, since the best estimate fine-group spectra from the eight different cuts are used to prepare the equivalent cross sections. The effects of approximations made in

the other models will therefore be determined by comparison with this reference model and the reference results provided.

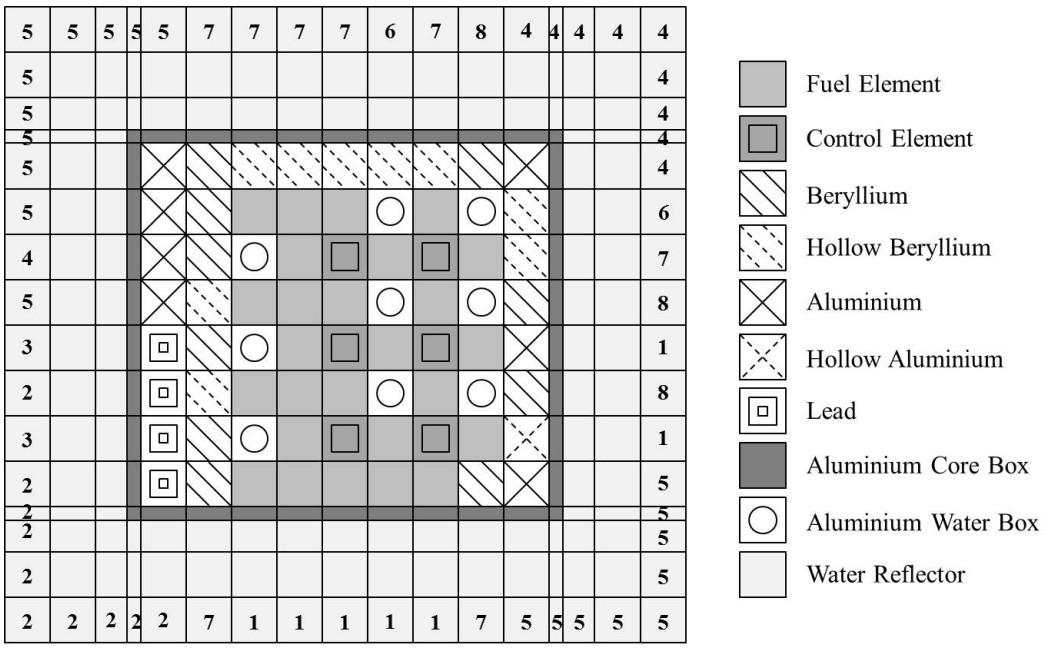

Figure 6.1: SAFARI-1 model with eight 1D models for the reflector representation

The reference model is based on the actual SAFARI-1 cycle C1001-1 history, as described in Section 3.2.2. This core is burnt for a period of 30 days, and a critical rod-search is performed, in order to determine the critical control bank positions at all the burnup steps for the duration of the cycle. Table 6.1 contains a description of the time-steps used for burn-up, the k_{eff} and the critical bank positions. These critical bank positions, are used in all the subsequent core calculations.

Neutron leakage plays an important role in small MTR reactors. Table 6.2 provides a summary of the neutron leakage from the core. This data shows that the radial leakage is more than twice as high as the axial leakage, and the non-thermal leakage is by far the greatest contributor to the radial leakage. Recall from Chapter 5 that the reflector response matrices showed some sensitivity to the core environment, mainly in the thermal energies. This finding indicates that the environment-sensitivity of the reflector response matrices might not have a large impact on a global scale.

Note that the leakage at beginning of cycle (BOC) and end of cycle (EOC) are similar in value. This is an indication that fuel burn-up does not have a large effect on the global leakage spectrum. The BOC U-235 mass is 7.873 kg (for the whole core). The EOC mass is 7.184 kg. This gives a burn-up of roughly 8.75 % (or 689 g) of the original U-235 mass during the cycle.

The assembly averaged power distribution at BOC and EOC is given in Tables 6.3 and 6.4 respectively. Here, the highest five values are indicated in green and the lowest five values are indicated in red. At BOC, the lowest power is produced in the control elements (positions C5, C7, E5, E7, G5 and G7). The control elements are 60 % extracted at BOC, so the fuel-followers attached to the bottom of the absorber are located in the lower half of the active core only. At EOC, the control elements are 87 % extracted and a greater part of the fuel-followers are in the active core. Therefore the core position with the lowest power has shifted away from the control elements towards the

Table 6.1: Cycle evolution for the reference core calculation

Time (days)	k-eff	Control bank (% inserted)
0.00	0.99998	39.9
0.09	0.99968	40.0
0.12	0.99938	39.9
0.95	0.99999	30.6
3.95	1.00036	29.1
6.95	0.99982	26.8
9.53	1.00000	24.8
9.53	0.99964	24.9
12.53	1.00045	22.9
15.54	0.99993	21.8
18.54	0.99997	20.7
21.54	1.00032	19.6
24.54	0.99973	17.0
27.54	0.99969	14.7
29.71	1.00020	13.0

Table 6.2: Leakage summary for the reference calculation

Leakage (%)	BOC	EOC
Total	25.82	25.42
Axial	7.29	6.92
Radial	18.53	18.50
Radial epi-thermal	20.56	20.51
Radial thermal	-2.03	-2.02

pool-side of the reactor (row H). The highest power is produced the furthest away from the pool-side (rows B and C) because here, the surrounding beryllium reflectors provide more neutrons for fission. The large effect of the core leakage, especially at the pool-side (below row H), can also be seen. Even though a fresh fuel element was loaded in position H3 at BOC, the power produced in this element is low, compared to the other fuel elements.

The assembly averaged thermal flux (sum of energy groups 5 and 6 in Table 3.1) distribution at BOC and EOC is given in Tables 6.5 and 6.6. Only the in-core position values are shown. This study only focuses on the in-core results, since the ex-core reflector regions will be represented by different models that do not facilitate comparisons. Furthermore, since the ex-core regions are represented by NGET ENPs, where the cross-sections are divided by the single normalised discontinuity factor, the ex-core flux values are not physical.

The highest and lowest ten values are indicated in green and red respectively. For clarity, the active core is indicated by a bold frame. The highest thermal flux in the core is found in the region surrounding the water-filled aluminium structural elements in the core (positions C3, E3 and G3). These water boxes act as thermal flux traps, since they are filled with a neutron moderator (water).

Table 6.3: Reference assembly averaged power distribution at BOC

I/J	1	2	3	4	5	6	7	8	9
A									
B			3.40	3.08	3.72		3.63		
C				3.98	2.42	3.86	2.40	3.33	
D			4.14	3.89	3.38		3.66		
E				3.65	2.05	3.42	2.30	2.94	
F			3.75	3.40	3.29		3.27		
G				3.48	1.81	3.10	2.17	2.73	
H			2.94	2.76	2.79	2.69	2.57		

Table 6.4: Reference assembly averaged power distribution at EOC

I/J	1	2	3	4	5	6	7	8	9
A									
B			2.94	2.78	3.58		3.64		
C				3.65	2.81	3.98	2.81	3.50	
D			3.55	3.54	3.36		3.91		
E				3.36	2.42	3.58	2.77	3.17	
F			3.24	3.11	3.30		3.53		
G				3.25	2.15	3.24	2.58	2.95	
H			2.57	2.55	2.76	2.72	2.70		

Table 6.5: Reference thermal flux distribution at BOC ($\times 10^{12}$)

I/J	1	2	3	4	5	6	7	8	9
A	1.78	2.70	2.93	2.03	5.65	5.38	4.28	3.41	2.20
B	2.26	4.00	3.87	4.12	4.79	6.37	3.98	4.45	3.39
C	2.72	5.31	6.68	5.49	4.89	5.48	3.84	3.79	4.11
D	3.06	5.77	5.82	6.30	6.88	7.76	5.20	5.42	4.34
E	3.50	6.69	7.73	6.53	5.87	6.44	4.34	3.93	3.53
F	3.50	6.30	5.75	6.14	6.46	7.41	4.97	4.98	4.05
G	3.06	5.60	6.16	4.99	4.71	5.11	3.44	3.17	3.40
H	2.40	3.77	3.24	3.54	3.69	3.54	3.03	3.19	2.43

Table 6.6: Reference thermal flux distribution at EOC ($\times 10^{12}$)

I/J	1	2	3	4	5	6	7	8	9
A	4.91	7.42	8.10	5.77	16.87	16.65	13.44	10.90	7.10
B	6.21	11.01	10.69	11.77	14.56	19.99	12.57	14.29	11.04
C	7.49	14.69	18.70	16.09	16.64	17.74	13.45	12.35	13.52
D	8.44	16.03	16.43	18.57	22.04	25.50	17.24	18.04	14.49
E	9.69	18.67	21.91	19.59	20.58	21.53	15.69	13.13	11.80
F	9.71	17.60	16.36	18.28	20.92	24.57	16.67	16.75	13.62
G	8.49	15.63	17.46	14.83	16.31	16.76	12.25	10.47	11.35
H	6.67	10.53	9.11	10.30	11.34	11.05	9.69	10.48	8.06

6.2 Reflector homogenisation

In this section, the effect of reflector homogenisation is discussed. The same configuration with all eight 1D reflector cuts are used as in the reference model, with the exception of the two inner

reflector nodes that have been homogenised and are thus modelled as a single node. Figure 6.2 illustrates this model of SAFARI-1. A summary of the results, as compared with the reference model, is discussed below. Further comparisons are included in Appendix D.

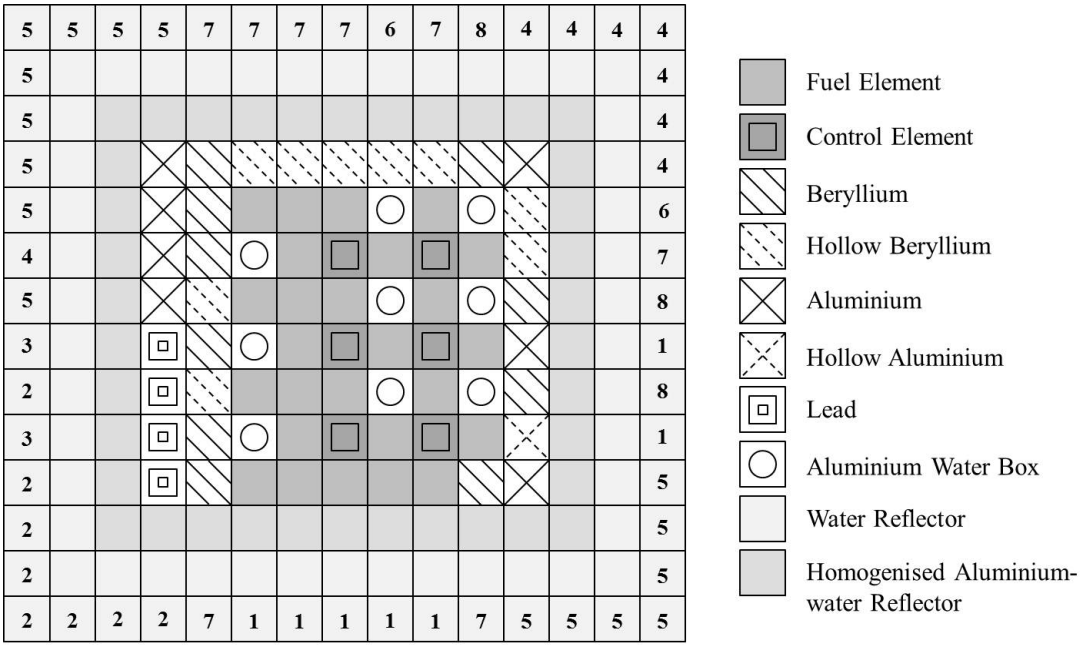

Figure 6.2: SAFARI-1 model with homogenised reflector and eight 1D reflector cuts

The k_{eff} of this new model is compared to that of the reference model. The reactivity difference is measured in pcm, which is calculated as:

$$\delta\rho = \frac{k_1 - k_2}{k_1 k_2} \times 10^5.$$

This comparison can be found in Table D.1. On average, the k_{eff} for this model is 40 pcm higher than in the reference model. The results also show that the reactivity difference remain constant throughout the cycle. Table D.2 compares the differences in the total neutron leakage and leakage spectrum of these two models. The leakage spectrum is not significantly affected by the change in the reflector model. The difference in leakage is less than 1 % at BOC and EOC. The slight decrease in all the leakage values is consistent with the small increase in the core reactivity (the 40 pcm increase in the calculated k_{eff}).

Differences in leakage, as well as power and flux (to follow) are calculated in percentage relative difference. For example, the percentage relative error in power in node i is:

$$\delta_{P_i} = \frac{P_i - P_{\text{ref}}}{P_{\text{ref}}} \times 100.$$

Next, the assembly averaged power distribution through the core is discussed. Tables 6.7 and 6.8 show the difference in power distribution between the reference model and the homogenised model, at BOC and EOC respectively. Colour has been added to the results, to highlight the biggest differences. The differences greater than 0.5 % and smaller than -0.5 % are indicated in dark green

and dark red respectively. Differences of between 0.25 % and 0.5 % are indicated in light green, and differences between −0.5 % and −0.25 % are marked in light red. This colour scheme is used for all power comparisons presented in this work.

The biggest difference in power is observed in positions H4 and H5, at BOC, where the homogenised model shows an 0.72 % increase in power relative to the reference model. At BOC and EOC, an increased power is observed at the pool-side of the core. Here the fuel elements are in close proximity to the homogenised reflector and is more sensitive to a change in reflector cross-sections. The increase in power at the pool-side, is balanced by a decrease in power at the opposite side of the core, because the total core power remains at 20 MW.

Table 6.7: Effect of homogenisation on the core model: power at BOC

I/J	1	2	3	4	5	6	7	8	9
A									
B			-0.59	-0.32	0.00		0.00		
C				-0.50	0.41	-0.26	0.42	0.00	
D			-0.24	-0.26	-0.30		0.00		
E				0.00	0.49	0.00	0.43	0.00	
F			0.00	0.00	0.00		0.00		
G				0.00	0.00	0.00	0.46	-0.37	
H			0.68	0.72	0.72	0.37	0.39		

Table 6.8: Effect of homogenisation on the core model: power at EOC

I/J	1	2	3	4	5	6	7	8	9
A									
B			-0.68	0.00	0.00		0.27		
C				-0.27	0.00	-0.25	0.00	0.00	
D			0.00	-0.28	0.00		0.00		
E				0.00	0.00	0.00	0.00	0.00	
F			0.00	0.00	0.00		0.00		
G				0.00	0.00	0.00	0.00	-0.34	
H			0.39	0.39	0.36	0.37	0.37		

Results for BOC and EOC thermal flux distribution, as compared to the reference model, are given in Tables 6.9 and 6.10. A different colour scheme is used for the flux results. Here, dark green indicates differences larger than 2 % and dark red indicates differences smaller than −2 %. Light green and light red indicate differences of between 0.5 % and 2 % and between −2 % and −0.5 % respectively. This colour scheme is used for all flux comparisons presented in this work. For clarity, the active core is indicated with a bold frame.

In the active core, the difference in thermal flux is less than 1 % at BOC and EOC. Differences are bigger in the reflectors surrounding the fuel. Here, the largest differences are observed in the corners of the model, with the maximum difference of 9.59 % in the top left hand corner (position A1). The corner regions are surrounded by the reflector on two sides and one would expect the differences to be larger. The differences are also typically larger for assembly positions further from the core, since the diffusion equation may not be very accurate in these outer regions.

Table 6.9: Effect of homogenisation on the core model: thermal flux at BOC

I/J	1	2	3	4	5	6	7	8	9
A	-9.52	-1.92	1.46	0.82	1.46	2.55	2.40	0.98	-1.42
B	-5.31	-1.77	-0.36	-0.08	0.10	0.01	0.35	0.87	1.05
C	-2.74	-1.08	-0.41	-0.10	-0.01	0.21	0.24	0.42	1.66
D	-1.45	-0.70	-0.22	-0.03	0.10	0.18	0.36	0.41	0.63
E	-0.81	-0.28	-0.16	0.03	0.13	0.28	0.32	0.30	-0.42
F	-0.35	-0.18	0.01	0.14	0.26	0.30	0.44	0.26	-1.46
G	-0.55	0.07	0.10	0.23	0.29	0.38	0.40	0.13	-3.80
H	-2.54	0.96	0.63	0.72	0.78	0.80	0.74	-1.08	-8.69

Table 6.10: Effect of homogenisation on the core model: thermal flux at EOC

I/J	1	2	3	4	5	6	7	8	9
A	-9.59	-1.85	1.57	0.82	1.54	2.57	2.41	0.98	-1.44
B	-5.31	-1.63	-0.20	0.00	0.09	-0.01	0.26	0.85	1.03
C	-2.73	-0.96	-0.28	-0.07	-0.02	0.08	0.17	0.31	1.62
D	-1.43	-0.60	-0.13	-0.03	0.01	0.06	0.17	0.31	0.57
E	-0.81	-0.20	-0.09	0.00	0.03	0.10	0.17	0.12	-0.48
F	-0.39	-0.15	0.02	0.07	0.09	0.11	0.18	0.10	-1.53
G	-0.66	0.05	0.07	0.09	0.10	0.12	0.16	-0.13	-3.93
H	-2.86	0.69	0.32	0.41	0.48	0.51	0.44	-1.32	-8.92

Results show that homogenised ENPs for the reflector are not sensitive to the fuel burn-up. This is seen in the comparisons for k_{eff}, leakage from the core and in power and thermal flux values. This model compares reasonably well with the reference model, with an average of 40 pcm higher reactivity and less than 1 % difference in power and flux in the active core. However, the flux values in the corners of the core differ with almost 10 % from the reference. The fact that the corner reflector assemblies face the ex-core reflector on two sides, introduces much larger reflector homogenisation effects. This may also indicate some 2D effects that cannot be modelled with the current approach. In PWR appllications [6] these 2D effects were however mainly applicable to inner corners, and not really at outer corners, as is the case here.

6.3 Reflector size reduction

In this section, the effect of reducing the reflector ex-core region to a single node, followed by an NGET albedo boundary condition, is investigated. Figure 6.3 represents this model, which has a reduced size compared to the full model. The ex-core reflector was modelled as four different nodes in the reference model (the core-box and three water regions) and as three nodes in the homogenised representation (homogenised core-box and water, followed by the two outer water regions). Here, only the single node representing the ex-core reflector is modelled.

In order to investigate the effect of reflector size reduction on the model, the reduced model is first compared to the homogenised model. These comparisons determine the accuracy of replacing the two outer water nodes with an NGET albedo boundary condition. The results are discussed in Section 6.3.1, and all the detailed comparisons are given in Appendix D. Secondly, the reduced

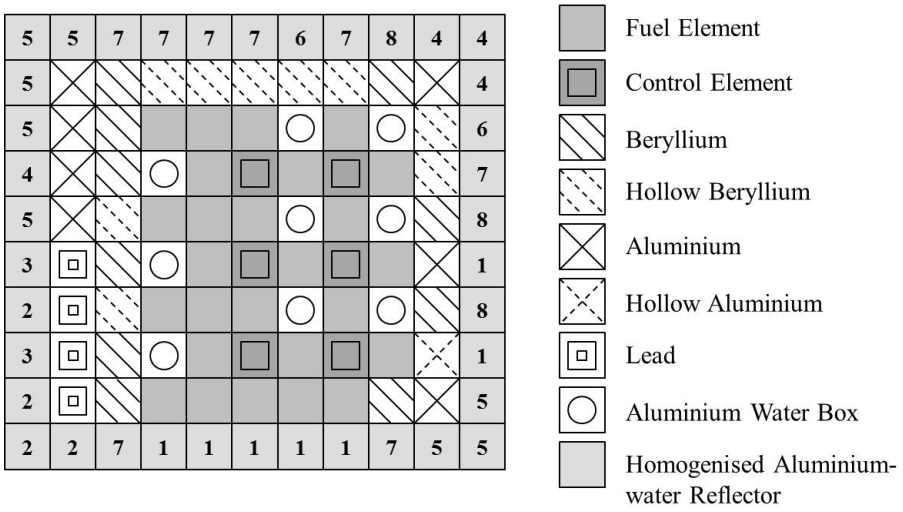

Figure 6.3: SAFARI-1 model with reduced reflector and eight reflector cuts

reflector representation results are compared with the reference model results, in Section 6.3.2. This evaluates the combined effects of homogenisation and reflector model reduction.

The reduction in the overall size of the core model is one of the main objectives of this work. This should result in a much faster and more stable (iteratively) solution, since less time is spent on solving for the neutron flux in the reflector regions far from the core. A significant CPU time reduction is therefore expected.

6.3.1 Effect of size reduction

Comparisons between the homogenised reflector model (Figure 6.2) and the reduced reflector model (Figure 6.3) are given in Tables D.3 to D.8. These comparisons indicate that the size reduction of the reflector increases the reactivity with 37 pcm and changes the power per assembly with at the most 1.66 %. The flux in the active core changes with at the most 1.75 % and at the most 2.2 % in the surrounding reflector assemblies. These results indicate that a reduction in reflector size does not introduce errors due to corner effects.

6.3.2 Effect of homogenisation and size reduction

In this section, the reduced model (Figure 6.3) is directly compared to the reference model (Figure 6.1). The k_{eff} of the reduced model is higher than that of the reference model. An average increase of 78 pcm is observed (see Table D.9). Less than 0.5 % differences are observed in the leakage spectra of the two core models. Again, the fuel burn-up throughout the cycle does not influence the reactivity or leakage differences between the models.

Tables 6.11 and 6.12 show the difference in power distribution between the reference model and the reduced model, at BOC and EOC respectively. As was the case in Section 6.2, larger differences in assembly power (roughly 0.8 %) are found at the pool-side of the core, because in this region,

the fuel is adjacent to the ex-core reflector and thus more sensitive to changes in reflector cross-sections.

Table 6.11: Effect of homogenisation and size reduction on the core model: power at BOC

I/J	1	2	3	4	5	6	7	8	9
A									
B			-0.88	-0.65	-0.54		-0.55		
C				-0.75	1.24	-0.52	1.25	0.00	
D			-0.72	-0.51	-0.59		-0.27		
E				-0.27	1.46	-0.29	1.74	0.00	
F			-0.27	-0.29	-0.30		0.00		
G				0.00	1.66	0.00	1.38	-0.37	
H			0.34	0.72	0.72	0.74	0.39		

Table 6.12: Effect of homogenisation and size reduction on the core model: power at EOC

I/J	1	2	3	4	5	6	7	8	9
A									
B			-0.68	-0.36	0.00		0.00		
C				-0.55	-0.36	-0.25	0.00	0.00	
D			-0.28	-0.28	0.00		-0.26		
E				0.00	0.00	0.00	0.00	0.32	
F			0.00	0.00	0.00		0.00		
G				0.00	0.00	0.31	0.00	0.00	
H			0.39	0.78	0.72	0.74	0.37		

Table 6.13: Effect of homogenisation and size reduction on the core model: thermal flux at BOC

I/J	1	2	3	4	5	6	7	8	9
A	-7.73	-1.45	1.51	1.35	1.49	2.56	2.45	1.02	-1.41
B	-4.07	-1.35	0.13	0.65	0.85	0.59	1.23	1.37	1.19
C	-1.84	-0.79	-0.05	0.63	0.53	1.27	0.95	1.46	2.13
D	-0.78	-0.44	0.29	0.77	1.02	1.16	1.63	1.44	1.73
E	-0.45	-0.12	0.22	0.80	0.80	1.44	1.24	1.78	1.50
F	-0.19	-0.03	0.57	1.02	1.31	1.40	1.84	1.50	0.28
G	-0.52	0.17	0.60	1.22	1.13	1.71	1.40	1.58	-2.15
H	-2.89	0.83	1.48	2.10	2.37	2.56	2.30	-0.13	-7.07

Table 6.14: Effect of homogenisation and size reduction on the core model: thermal flux at EOC

I/J	1	2	3	4	5	6	7	8	9
A	-7.60	-1.21	1.74	1.31	1.61	2.59	2.45	1.02	-1.38
B	-3.87	-1.04	0.37	0.64	0.62	0.37	0.81	1.18	1.13
C	-1.63	-0.50	0.16	0.52	0.39	0.68	0.66	0.97	1.99
D	-0.56	-0.18	0.41	0.59	0.56	0.62	0.88	0.99	1.54
E	-0.26	0.12	0.36	0.61	0.50	0.76	0.79	1.10	1.26
F	-0.03	0.16	0.61	0.77	0.77	0.78	1.00	0.94	0.04
G	-0.43	0.30	0.64	0.94	0.75	0.99	0.91	0.86	-2.41
H	-3.01	0.72	1.25	1.70	1.80	1.88	1.58	-0.61	-7.34

The largest differences are found in the control assemblies at BOC, where the power in the reduced model is up to 1.74 % higher than in the reference model. However, these relative differences

Table 6.15: The calculational time for three different models of SAFARI-1

Model	Time (minutes)	Difference (minutes)
Reference model	26.9	
Homogenised reflector	20.7	-6.1
Homogenised and reduced reflector	12.2	-14.7

are calculated for the numerically small control assembly powers at BOC, when the control rods are half-way inserted. Therefore these differences are not very significant. This is supported by the EOC results, where no differences are observed. At EOC, the control rods are almost fully extracted and the power in the control positions are more or less the same as in the fuel positions.

Tables 6.13 and 6.14 show the difference in thermal flux distribution between the reference model and the reduced model, at BOC and EOC respectively. The maximum difference in the active core is 2.56 % at the pool-side, at BOC. Except for this row, the difference in flux in the active core does not exceed 2 %. However, the surrounding reflectors have differences of up to 7.73 %, with the largest differences in the corner nodes. The EOC flux difference distributions behave similar than at BOC.

In summary, the reduced reflector model is not sensitive to the fuel burn-up during the cycle calculation. Differences in power and flux distribution appear to be caused mainly by homogenisation, and not by size reduction. The differences observed in flux and power, due to the homogenisation of the reflector nodes (higher power at pool-side and lower flux in corners) are also observed in this model comparison. Additional to this, size reductions cause some differences in the power in the control elements, at BOC.

As mentioned in the beginning of this section, one of the reasons for a reduction in reflector size, is the reduced number of calculational nodes in a smaller model. The reduced model will be much faster to compute, exactly because of the reduction in the number of calculations to perform. Convergence behaviour of the code will also be better for a model with a smaller reflector. Table 6.15 gives the time it took to complete the 30 day cycle simulation for the three models described in Sections 6.1 to 6.3. These results prove that the reduced model takes the least amount of time to run, less than half the time that the reference, explicit model takes. This is a significant improvement. Specifically if multiple reload studies need to be performed, or if reload optimization, that needs hundreds of these runs, is to be practically achievable.

6.4 Sensitivity to the fuel driver zone

In this section, the sensitivity of the reflector ENPs to the fuel driver zone characteristics (or model choices) is investigated. First, the reflector's sensitivity to fuel burn-up in the driver zone is quantified. Thereafter follows a discussion on the sensitivity of the reflector ENPs to fuel orientation, number of fuel elements defined in the model, and the enrichment of the fuel driver zone.

Table 6.16: Effect of burnup in fuel driver zone: power at BOC

I/J	1	2	3	4	5	6	7	8	9
A									
B			0.00	-0.33	0.00		0.00		
C				0.00	-0.41	-0.26	0.00	-0.30	
D			0.00	-0.26	0.00		0.00		
E				-0.27	0.00	0.00	0.00	0.00	
F			0.00	0.00	0.00		0.00		
G				0.00	0.00	0.00	0.00	0.37	
H			0.34	0.36	0.36	0.37	0.39		

Table 6.17: Effect of burnup in fuel driver zone: power at EOC

I/J	1	2	3	4	5	6	7	8	9
A									
B			0.00	0.00	-0.28		0.00		
C				0.00	0.00	0.00	0.00	0.00	
D			0.00	0.00	-0.30		0.00		
E				-0.30	0.00	0.00	0.00	0.00	
F			0.00	0.00	0.00		0.00		
G				0.00	0.00	0.00	0.39	0.00	
H			0.39	0.39	0.36	0.36	0.37		

Table 6.18: Effect of burnup in fuel driver zone: thermal flux at BOC

I/J	1	2	3	4	5	6	7	8	9
A	0.22	0.04	-0.04	-0.08	-0.10	-0.08	-0.06	-0.04	0.02
B	0.12	-0.04	-0.10	-0.12	-0.12	-0.11	-0.10	-0.08	-0.01
C	0.07	-0.05	-0.10	-0.11	-0.11	-0.10	-0.10	-0.08	0.02
D	0.06	-0.04	-0.08	-0.09	-0.09	-0.09	-0.08	-0.04	0.11
E	0.05	-0.03	-0.05	-0.06	-0.06	-0.06	-0.05	0.00	0.27
F	0.08	0.02	-0.01	-0.01	-0.02	-0.01	-0.01	0.04	0.25
G	0.16	0.09	0.06	0.05	0.04	0.04	0.05	0.09	0.33
H	0.39	0.33	0.27	0.28	0.28	0.28	0.28	0.43	0.66

Table 6.19: Effect of burnup in fuel driver zone: thermal flux at EOC

I/J	1	2	3	4	5	6	7	8	9
A	0.24	0.05	-0.02	-0.05	-0.08	-0.06	-0.05	-0.02	0.04
B	0.13	-0.02	-0.09	-0.10	-0.10	-0.09	-0.09	-0.06	0.00
C	0.08	-0.04	-0.08	-0.09	-0.10	-0.09	-0.08	-0.07	0.04
D	0.06	-0.03	-0.07	-0.08	-0.08	-0.08	-0.08	-0.03	0.12
E	0.05	-0.03	-0.05	-0.06	-0.06	-0.06	-0.05	0.00	0.28
F	0.07	0.01	-0.02	-0.02	-0.02	-0.02	-0.01	0.03	0.24
G	0.15	0.08	0.05	0.03	0.03	0.03	0.03	0.07	0.32
H	0.38	0.32	0.25	0.26	0.25	0.25	0.25	0.40	0.64

The SAFARI-1 fuel elements in any core are on average burnt between 20 and 30 % (of U-235 mass), and the maximun fuel burnup is around 60 %. For this study, a fuel burnup of 40 % of U-235 is chosen. A second reduced core model is defined as before (Figure 6.3), except that the reflector ENPs are prepared using a burnt fuel driver zone, whereas a fresh fuel definition was used

before. Therefore, the only difference between the two models is the fuel isotopic composition in the 1D reflector models (fresh and burnt fuel). This model is compared to the reduced model from the previous section.

Tables D.11 and D.12 in Appendix D show the difference in k_{eff} and leakage from the core between these two models. The k_{eff} for the model with a burnt fuel driver zone is on average only 12 *pcm* higher than for the reduced model with a fresh fuel driver zone. No diffference is observed in the overall leakage or leakage spectrum between these two models.

Tables 6.16 and 6.17 illustrate differences in power distribution at BOC and EOC, and Tables 6.18 and 6.19 show differences in thermal flux distribution at BOC and EOC respectively. All these results indicate that the burn-up in the fuel driver zone of the reflector models, do not have a noticable global effect on the reactor ENPs. This result confirms the previous comparisons that have shown almost no difference between BOC and EOC.

In previous studies [50, 51] it were also found that the reflector ENPs are not sensitive to the fuel burnup. Other results from [50] showed that the reflector ENPs are also not very sensitive to fuel enrichment (where high enriched uranium and low enriched uranium were used in fuel driver zones) or to the orientation of the fuel plates in the fuel driver zone. This last finding is important for the present study, because the fuel plates in SAFARI-1 are all orientated in the same direction, which is parallel to the pool-side face of the core. This finding indicates that the same ENPs can be used on all sides of the reactor. This last finding was confirmed in the present study, where a rotated model was created and used for the top and bottom axial reflectors. The effect was negligible.

A small dependence of the reflector ENPs on the number of fuel elements in the driver zone was observed in [50], when two fuel elements, instead of one, were used as the fuel driver zone. This dependency was observed in the comparison of albedo values for different 1D reflector models. The global importance of this dependency has not been established. However, in the checkerboard layout of the SAFARI-1 reactor this dependency will come into effect, and is not investigated further.

6.5 Environment sensitivity of the reflector

In this section, the sensitivity of the reflector to the core environment is determined. In Sections 6.1 to 6.4, eight different reflector cuts were used to model the reflector in full-core calculations. Here, an attempt is made to simplify the reflector model, by using only one or two reflector cuts, instead of all eight, to model the reflector. Further simplification of the reflector model is obtained by using the homogenised and reduced reflector models, instead of the explicit ones. A summary of the results, as compared with the reference model, is discussed below. Further comparisons are included in Appendix E.

6.5.1 Explicit model with one reflector cut

In this section, only Cut 1 (see Figure 3.5) is used to represent the whole reflector. This core is modelled with an explicit reflector, as illustrated in Figure 6.4. Results are compared to the reference model (Figure 6.1).

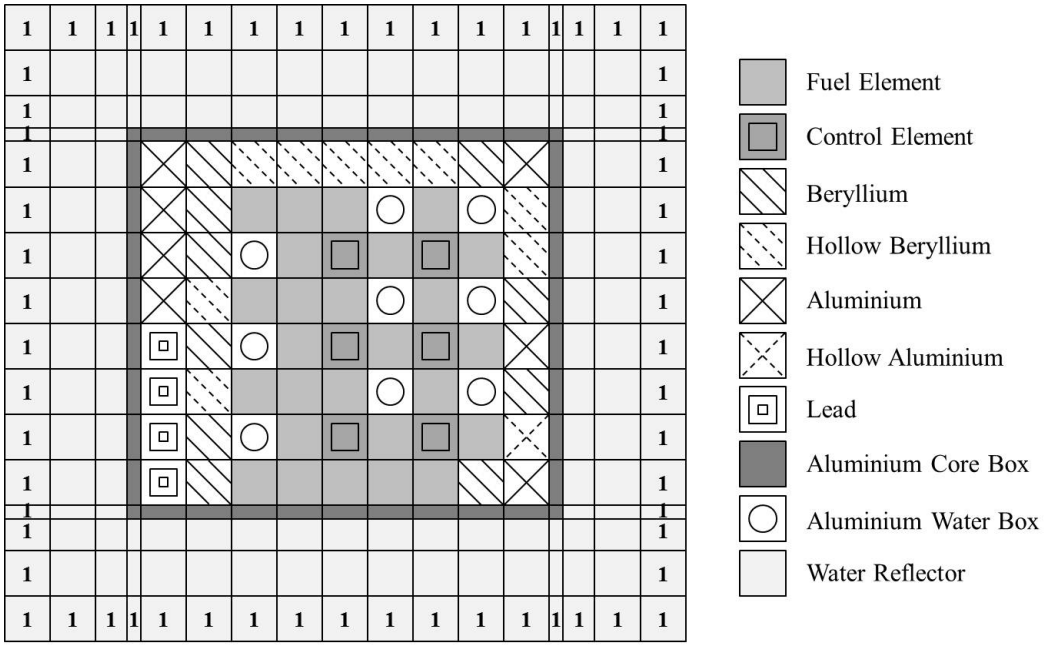

Figure 6.4: SAFARI-1 model with explicit reflector and one reflector cut

Comparisons between the reference model and this explicit model are given in Tables 6.20 to 6.23. Extra detail is given in Tables E.5 and E.6. Rather large differences are observed. This new explicit model increases the k_{eff} with an average of 196 pcm. The thermal leakage from the core is about 5 % higher than for the reference model. This finding is expected, since Cut 1, which is used for the reflector representation, has no in-core reflectors to reduce the neutron leakage out of the core.

Power differences are not so large, with a maximum difference of 1.2 %. Flux differences are mostly less than 1 % in the fuel, except in the corners, but increase to almost 12 % difference in the corners of the core.

Note the power tilt introduced by this model. In all the previous models, slight power tilts were seen parallel to the pool-side of the core (i.e. a top-bottom tilt), but here, a power tilt is observed perpendicular to the pool-side of the core (i.e. left-right tilt). At the left and right sides of the core the fuel is the furthest away from the ex-core reflector. Cut 1 is a poor approximation for these areas of the reflector, which explains why the largest differences are found on these sides of the core.

Table 6.20: Effect of using one explicit reflector model for all reflector nodes: power at BOC

I/J	1	2	3	4	5	6	7	8	9
A									
B			0.29	0.00	0.27		1.10		
C				-0.25	0.00	-0.26	0.42	1.20	
D			-0.24	-0.51	-0.59		0.00		
E				-0.55	-0.49	-0.29	0.00	0.68	
F			0.00	-0.59	-0.61		0.00		
G				-0.29	-0.55	-0.32	0.00	0.73	
H			0.68	0.00	0.00	0.00	0.78		

Table 6.21: Effect of using one explicit reflector model for all reflector nodes: power at EOC

I/J	1	2	3	4	5	6	7	8	9
A									
B			0.00	0.00	0.28		1.10		
C				-0.55	-0.36	-0.25	0.00	0.86	
D			0.00	-0.56	-0.30		0.00		
E				-0.30	-0.41	-0.28	-0.36	0.95	
F			-0.31	-0.32	-0.30		-0.28		
G				-0.31	-0.47	0.00	0.00	0.68	
H			0.39	0.00	0.00	0.00	0.74		

Table 6.22: Effect of using one explicit reflector model for all reflector nodes: thermal flux at BOC

I/J	1	2	3	4	5	6	7	8	9
A	7.08	4.29	2.94	2.34	2.06	3.28	4.56	6.62	11.90
B	5.37	1.98	0.38	0.06	0.25	0.78	1.10	2.72	6.60
C	4.70	1.27	0.06	-0.24	-0.26	0.01	0.25	1.18	4.59
D	4.35	1.07	-0.16	-0.40	-0.38	-0.22	0.09	1.02	3.69
E	3.86	0.77	-0.17	-0.45	-0.50	-0.30	-0.10	0.82	3.86
F	3.96	0.89	-0.15	-0.42	-0.43	-0.30	-0.02	0.81	2.97
G	4.78	1.27	0.14	-0.25	-0.38	-0.20	0.06	0.85	2.98
H	6.61	2.69	0.72	0.16	0.02	0.22	0.79	2.59	5.05

Table 6.23: Effect of using one explicit reflector model for all reflector nodes: thermal flux at EOC

I/J	1	2	3	4	5	6	7	8	9
A	7.09	4.32	2.97	2.34	2.02	3.19	4.47	6.52	11.80
B	5.36	1.95	0.34	0.00	0.20	0.70	1.04	2.63	6.51
C	4.67	1.24	0.03	-0.28	-0.26	-0.04	0.24	1.13	4.51
D	4.32	1.04	-0.19	-0.43	-0.40	-0.24	0.06	0.97	3.62
E	3.83	0.75	-0.19	-0.48	-0.48	-0.32	-0.07	0.80	3.82
F	3.93	0.86	-0.16	-0.44	-0.44	-0.30	-0.02	0.79	2.92
G	4.75	1.24	0.11	-0.28	-0.36	-0.20	0.10	0.85	2.96
H	6.57	2.65	0.68	0.12	0.00	0.21	0.81	2.61	5.06

6.5.2 Reduced model with one reflector cut

In this section, Cut 1 (see Figure 3.5) is still used to represent the whole reflector. However, the core is now modelled with a reduced reflector, as illustrated in Figure 6.5. Results are compared to the reference model (Figure 6.1).

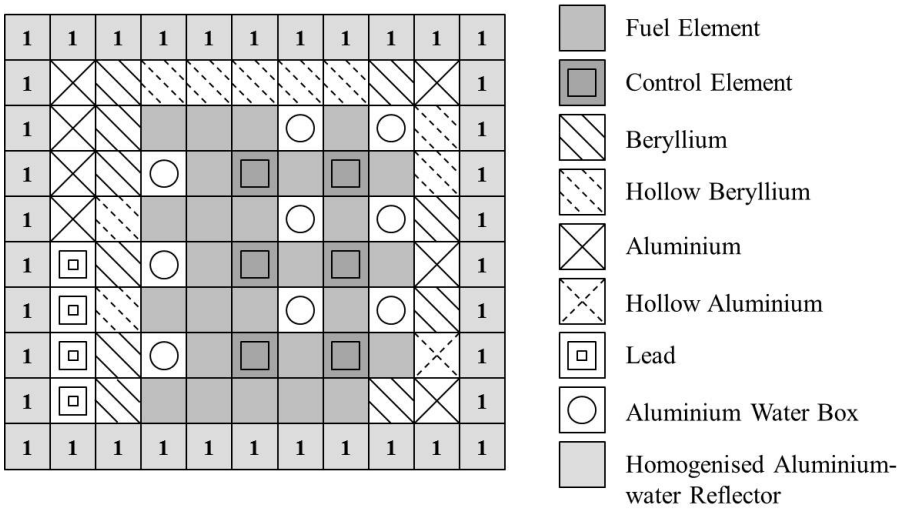

Figure 6.5: SAFARI-1 model with reduced reflector and one reflector cut

This model shows much smaller differences to the reference model, than the explicit reflector in Section 6.5.1 did. This suggests some fortunate cancellation of errors. Tables E.3 and E.4 show that this model causes almost no difference in the core reactivity, with an average increase of only 5 pcm. Roughly 5 % decrease in thermal leakage from the core is observed.

Tables 6.24 and 6.25 show that the difference in power distribution at BOC and EOC respectively, is less than 1.2 %, with a visible tilt across the core in the left-right direction. This tilt is in the opposite direction than the tilt observed for the previous model (Section 6.5.1). This suggests that the effects of homogenisation and size reduction on Cut 1 ENPs are rather large, in order to have such a noticable effect on the global core-calculation.

Table 6.24: Effect of using one reduced reflector model for all reflector nodes: power at BOC

I/J	1	2	3	4	5	6	7	8	9
A									
B			-0.59	-0.32	-0.27		-1.10		
C				-0.25	0.00	-0.26	0.00	-0.90	
D			-0.24	0.00	0.00		0.00		
E				0.00	0.49	0.29	0.43	-0.68	
F			0.00	0.29	0.30		0.00		
G				0.29	0.55	0.32	0.46	-0.73	
H			0.00	1.09	1.08	1.12	0.00		

Table 6.25: Effect of using one reduced reflector model for all reflector nodes: power at EOC

I/J	1	2	3	4	5	6	7	8	9
A									
B			-0.68	0.00	0.00		-0.55		
C				-0.27	0.00	-0.25	0.00	-0.86	
D			0.00	0.00	0.00		-0.26		
E				0.00	0.00	0.00	0.00	-0.32	
F			0.00	0.32	0.30		0.00		
G				0.31	0.00	0.31	0.39	-0.68	
H			-0.39	0.78	1.09	0.74	0.00		

Table 6.26: Effect of using one reduced reflector model for all reflector nodes: thermal flux at BOC

I/J	1	2	3	4	5	6	7	8	9
A	-11.28	-4.97	-1.95	-2.14	-0.69	-1.24	-2.60	-5.13	-10.91
B	-6.48	-2.39	-0.42	-0.06	-0.12	-0.75	-0.64	-1.37	-5.07
C	-4.05	-1.42	-0.36	-0.08	-0.07	-0.09	-0.16	-0.61	-3.04
D	-3.07	-1.10	-0.15	0.01	0.04	0.03	0.00	-0.48	-2.57
E	-3.13	-0.72	-0.10	0.12	0.17	0.19	0.16	-0.31	-2.75
F	-3.37	-0.81	0.10	0.28	0.35	0.34	0.32	-0.20	-2.94
G	-4.53	-0.99	0.09	0.45	0.55	0.52	0.46	-0.22	-4.79
H	-8.89	-1.95	0.35	1.12	1.27	1.15	0.50	-2.84	-10.24

Table 6.27: Effect of using one reduced reflector model for all reflector nodes: thermal flux at EOC

I/J	1	2	3	4	5	6	7	8	9
A	-11.45	-5.05	-2.02	-2.21	-0.62	-1.15	-2.47	-5.01	-10.85
B	-6.53	-2.30	-0.29	0.07	-0.04	-0.66	-0.56	-1.27	-5.04
C	-4.08	-1.34	-0.24	0.02	0.00	-0.04	-0.09	-0.55	-3.01
D	-3.08	-1.03	-0.07	0.07	0.07	0.06	0.01	-0.43	-2.53
E	-3.16	-0.68	-0.05	0.14	0.17	0.17	0.15	-0.33	-2.70
F	-3.42	-0.81	0.09	0.26	0.29	0.28	0.25	-0.23	-2.94
G	-4.65	-1.02	0.06	0.36	0.42	0.40	0.33	-0.32	-4.83
H	-9.19	-2.22	0.07	0.89	1.07	1.00	0.34	-2.96	-10.33

Tables 6.26 and 6.27 illustrate the difference in thermal flux distribution at BOC and EOC respectively. Similar to the explicit model comparisons, the reduced model shows small differences in the fuel, but large differences of almost 12 % in the corners.

In summary, although this reduced reflector model (with one cut for all reflector parameters) do not cause large differences in power or in flux for the active core, the large flux differences in the corners of the core model may be too large to justify the use of this model. This depends on the application of the model. If accurate flux measurements are required in the in-core reflector nodes (for use in experiments or isotope irradiation), then this model is not accurate enough.

6.5.3 Explicit model with two reflector cuts

The extra in-core reflector material and core-box in the corners of the core, appear to have a big impact on the reflector model. Based on this observation, another calculational model is suggested. For this model, two cuts are used to represent the whole reflector. These cuts are Cut 1 and Cut 7 (see Figure 3.5). Cut 1 is used only at the pool-side, where the fuel is adjacent to the reflector. Cut 7 is used everywhere else. This cut was selected as a good representation for the rest of the core; the fuel is some distance from the reflector (with hollow beryllium in-between) and most of the reflector around the core "see" hollow beryllium in the core.

This core is modelled with an explicit reflector, as illustrated in Figure 6.6. Results are compared to the reference model (Figure 6.1).

Comparisons between the reference model and this explicit model are given in Tables E.5 and E.6 in Appendix E and Tables 6.28 to 6.31. These two models compare extremely well. There is almost

no difference in reactivity (average increase of 3 pcm) or core leakage (maximum difference of 0.2 %). Less than 0.8 % difference is seen in the power distribution and thermal flux in the active core. Even in the corners, the flux differs with at the most 3.17 %. Evidently, this model is an excellent simplification of the reference model.

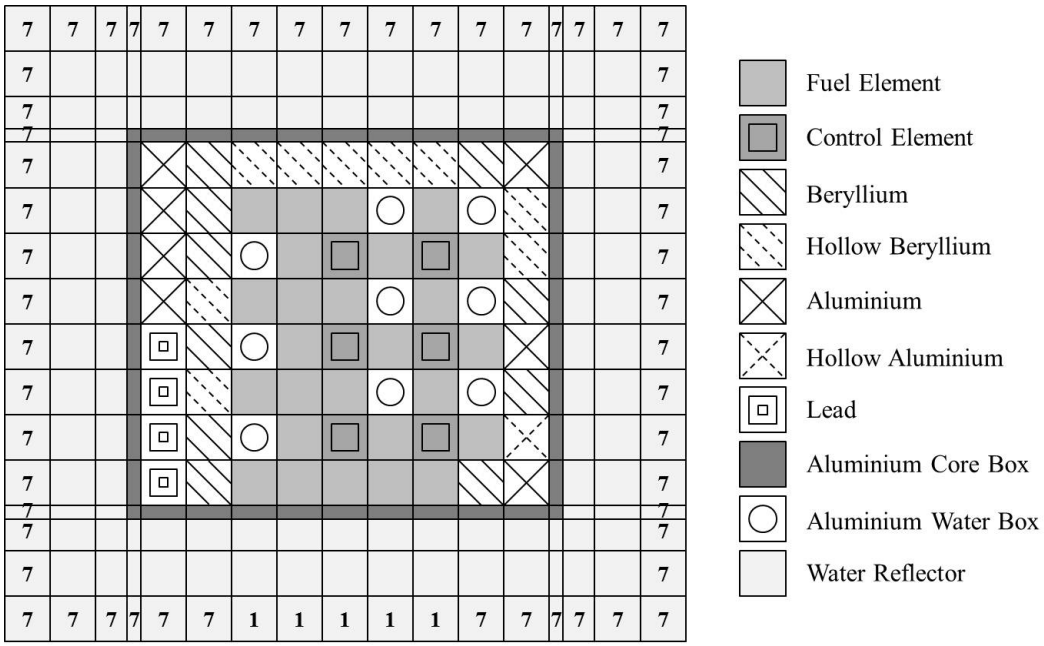

Figure 6.6: SAFARI-1 model with explicit reflector and two reflector cuts

Table 6.28: Effect of using two explicit reflector models for all reflector nodes: power at BOC

I/J	1	2	3	4	5	6	7	8	9
A									
B			0.29	0.00	0.27		0.28		
C				0.00	0.41	0.00	0.42	0.00	
D			0.24	0.00	0.00		0.00		
E				0.27	0.49	0.00	0.00	-0.34	
F			0.27	0.00	0.00		-0.31		
G				0.00	0.00	-0.32	0.00	-0.73	
H			0.00	0.00	0.00	-0.37	-0.39		

Table 6.29: Effect of using two explicit reflector models for all reflector nodes: power at EOC

I/J	1	2	3	4	5	6	7	8	9
A									
B			0.00	0.00	0.28		0.27		
C				0.00	0.00	0.00	0.00	0.00	
D			0.28	0.00	0.30		0.00		
E				0.00	0.00	0.00	-0.36	-0.32	
F			0.00	0.00	0.00		-0.28		
G				0.00	0.00	0.00	-0.39	-0.34	
H			0.00	0.00	0.00	-0.37	-0.37		

Recall from Chapter 5 that the response matrices for all the reflector cuts, except Cut 1, are very similar in value. Thus Cut 7 is expected to have a similar response on the core than all the other cuts

Table 6.30: Effect of using two explicit reflector models for all reflector nodes: thermal flux at BOC

I/J	1	2	3	4	5	6	7	8	9
A	-0.06	0.17	0.26	0.40	0.47	0.81	1.08	1.67	3.17
B	0.38	0.25	0.22	0.22	0.26	0.34	0.38	0.68	1.51
C	0.73	0.32	0.20	0.20	0.17	0.21	0.17	0.23	0.63
D	0.84	0.34	0.19	0.17	0.16	0.13	0.11	0.00	0.00
E	0.91	0.31	0.16	0.14	0.10	0.09	-0.01	-0.17	-0.63
F	0.94	0.31	0.14	0.11	0.08	0.02	-0.06	-0.29	-0.76
G	1.01	0.31	0.13	0.10	0.03	0.01	-0.12	-0.37	-1.23
H	0.96	0.34	0.14	0.09	0.04	-0.01	-0.14	-0.72	-1.78

Table 6.31: Effect of using two explicit reflector models for all reflector nodes: thermal flux at EOC

I/J	1	2	3	4	5	6	7	8	9
A	-0.05	0.17	0.26	0.40	0.46	0.79	1.06	1.66	3.16
B	0.39	0.26	0.22	0.21	0.24	0.31	0.35	0.65	1.49
C	0.73	0.32	0.20	0.19	0.17	0.18	0.16	0.20	0.62
D	0.86	0.35	0.20	0.16	0.13	0.10	0.07	-0.01	-0.01
E	0.92	0.33	0.18	0.14	0.09	0.06	-0.02	-0.20	-0.63
F	0.96	0.33	0.16	0.12	0.07	0.01	-0.08	-0.29	-0.74
G	1.04	0.33	0.16	0.10	0.05	0.00	-0.11	-0.37	-1.20
H	0.98	0.37	0.17	0.11	0.06	-0.01	-0.14	-0.70	-1.77

(except Cut 1). With this in mind, it is not difficult to understand why this two-cut-reflector model is such an accurate simplification of the reference eight-cut-reflector model. This also suggests that any of the other cuts (Cut 2 - Cut 8) could be used instead of Cut 7, with similar results, although this hypothesis has not been tested.

6.5.4 Reduced model with two reflector cuts

Finally, two-cut-reflector model is simplified even more. In this section, the same two reflector cuts are still used to represent the whole reflector, but the core is now modelled with a reduced reflector, as illustrated in Figure 6.7. Results are compared to the reference model (Figure 6.1).

As with the explicit model (discussed in Section 6.5.3), this model also compares well with the reference model. The reactivity increases with an average of 88 pcm for this model (see Table E.7). Leakages do not show a big difference, as illustrated in Table E.8. The maximum difference in leakage is 1.74 % in the thermal radial leakage. The thermal leakage is so small, that such a difference is negligible.

Tables 6.32 and 6.33 show the difference in power distribution at BOC and EOC respectively. Power distribution for this model differ with no more than 1.12 % from the reference model. The largest difference is seen at the pool-side of the core with a top-bottom power tilt. Since Cut 1 is used at the pool-side for both this model and the reference model, this power tilt is most likely caused by leakage differences across the other faces of the core. The power tilt is then caused by the redistribution (or renormalisation) of the powers to the total core power.

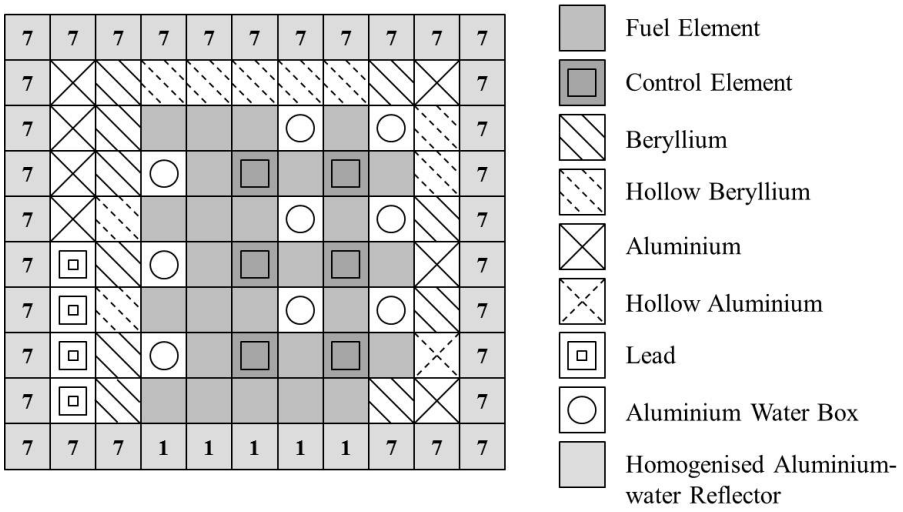

Figure 6.7: SAFARI-1 model with reduced reflector and two reflector cuts

Table 6.32: Effect of using two reduced reflector models for all reflector nodes: power at BOC

I/J	1	2	3	4	5	6	7	8	9
A									
B			-0.29	-0.65	-0.27		-0.28		
C				-0.50	-0.41	-0.52	0.00	0.00	
D			-0.24	-0.51	-0.59		0.00		
E				-0.27	0.00	0.00	0.00	0.68	
F			0.00	-0.29	0.00		0.00		
G				0.00	0.00	0.00	0.46	0.37	
H			0.68	1.09	1.08	1.12	0.78		

Table 6.33: Effect of using two reduced reflector models for all reflector nodes: power at EOC

I/J	1	2	3	4	5	6	7	8	9
A									
B			-0.34	-0.36	-0.28		0.00		
C				-0.55	-0.36	-0.25	0.00	0.00	
D			-0.28	-0.28	-0.30		-0.26		
E				-0.30	-0.41	0.00	0.00	0.63	
F			0.00	0.00	0.00		0.00		
G				0.00	0.00	0.31	0.00	0.34	
H			0.39	0.78	0.72	0.74	0.74		

The thermal flux distribution in this model compares excellent with that of the reference model (see Tables 6.34 and 6.35 for BOC and EOC flux differences respectively). The largest difference in the active core is 1.15 %. Furthermore, flux in the in-core reflectors differ with at most 3.59 %. The tables clearly illustrate that the differences in the corners are no larger than the differences anywhere else in the core.

To summarise, this model using two cuts to represent a reduced reflector model, compares very well with the reference model. A small increase (88 pcm) in reactivity is introduced, but differences of at most 1.12 % in power distribution and 3.59 % in thermal flux anywhere in the core, are introduced.

Table 6.34: Effect of using two reduced reflector models for all reflector nodes: thermal flux at BOC

I/J	1	2	3	4	5	6	7	8	9
A	-0.97	0.95	1.85	0.46	1.10	2.04	2.08	1.40	0.63
B	0.91	-0.02	-0.34	-0.38	-0.30	-0.38	-0.04	0.81	1.66
C	2.06	0.09	-0.39	-0.44	-0.43	-0.28	-0.16	0.22	2.35
D	2.46	0.21	-0.33	-0.37	-0.32	-0.23	-0.04	0.57	2.63
E	1.61	0.18	-0.22	-0.26	-0.22	-0.10	0.04	0.67	3.54
F	1.31	0.13	-0.07	-0.08	-0.01	0.06	0.24	0.77	2.16
G	0.98	0.32	0.13	0.14	0.19	0.26	0.38	0.64	0.62
H	-0.54	1.34	0.86	1.04	1.10	1.12	1.15	1.40	-0.63

Table 6.35: Effect of using two reduced reflector models for all reflector nodes: thermal flux at EOC

I/J	1	2	3	4	5	6	7	8	9
A	-1.09	0.95	1.89	0.46	1.18	2.10	2.15	1.45	0.66
B	0.87	0.07	-0.22	-0.27	-0.22	-0.32	0.01	0.87	1.68
C	2.01	0.15	-0.29	-0.36	-0.35	-0.23	-0.09	0.26	2.37
D	2.41	0.25	-0.27	-0.32	-0.29	-0.20	-0.02	0.60	2.64
E	1.55	0.19	-0.20	-0.25	-0.21	-0.11	0.04	0.67	3.59
F	1.21	0.10	-0.10	-0.12	-0.08	0.00	0.17	0.72	2.12
G	0.82	0.24	0.05	0.03	0.07	0.13	0.26	0.54	0.55
H	-0.91	1.01	0.52	0.76	0.87	0.97	1.01	1.31	-0.70

6.6 Summary of results

In this chapter, various calculational models for the SAFARI-1 reactor have been discussed. Results show that reflector homogenisation is sensitive to corner effects. As size reduction does not appear to share this sensitivity, it is concluded that homogenisation introduces the largest error in the reflector parameters. The calculational time is more than halved, if a reduced reflector model is used instead of the full explicit model. Any sensitivity that the reflector ENPs might have on the fuel driver zone, is negligible in the scale of global core-calculations.

The reflector equivalent nodal parameters show some sensitivity to the core environment. One set of ENPs can be used to represent the whole reflector, but errors are introduced, particularly near the corners of the model. By using two reflector cuts; one where the fuel is adjacent to the reflector, and another for the rest of the reflector, the reference results are reproduced to an acceptable accuracy. This model (illustrated in Figure 6.7) is smaller than the reference model, and a simplification thereof, with only two sets of ENPs for the reflector, instead of eight. Therefore less time is needed to run calculations with this model (recall Table 6.15) and the setup of this model is much simpler, without compromising on the accuracy of the model.

Chapter 7

Concluding remarks

A summary of the work performed and the results obtained are discussed in this chapter. Overhead conclusions are drawn and discussed. The last section in this chapter is a discussion on possible future work concerning reflector modelling in SAFARI-1.

7.1 Conclusion

The main objective of this work was to determine if normalised generalised equivalence theory is a practical method for MTR reflector modelling. The existing code EQUIVA-1 was used for this purpose to calculate equivalent nodal parameters for 1D reflector models. SCALE was used to calculate reference transport solutions for these reflector models. OSCAR-4 was used for all the other calculations (library creation for the rest of the core and full-core diffusion calculations).

A new calculational path has been established to calculate equivalent nodal parameters for reflector regions within the OSCAR-4 calculational system. This path links a reference transport code (SCALE 6.1) to the existing OSCAR-4 cross-section data handling modules. This newly established path was verified. A code-to-code comparison between SCALE and Serpent shows excellent agreement for a representative one-dimensional model. The calculational path was also verified, since equivalence was demonstrated between the transport and nodal diffusion solution in one-dimension, as per the theory. This confirms that the newly developed SCALE model and utility program to link it with OSCAR-4 works as intended.

The SAFARI-1 reactor (cycle C1001-1) was selected as the test case. The calculational model for the ex-core region consisting of the reactor core-box and surrounding water was investigated. From the detailed core layout, with its large number of different combinations of reflector elements and fuel environments, eight representative environments were selected to be representative of all the different reflector environments.

SCALE models representing a one-dimensional cut of these reflector environments were set up and detailed transport solutions were calculated in 238 energy groups. From the surface fluxes and

currents, the detailed fine-group albedos were calculated on selected surfaces. Results at the core-reflector boundary and after one reflector node, were presented. Large spectrum differences, and therefore large differences in the reflector albedos, are observed between the different cuts at the core reflector boundary. The differences are much smaller when the albedos after a single reflector node are compared. These results support the general practice not to define albedo boundary conditions directly on the core reflector interface, but rather some distance away from the core. The responses for the ex-core reflector region for the eight different cuts were calculated in EQUIVA-1 and evaluated. The reflective and transmission response matrices were compared. All the models except Cut 1 show similar results for both the transmission and reflection response matrices. Cut 1, where the fuel is directly adjacent to the core-box, sees a much harder neutron leakage spectrum than the other cases, where one or more reflector elements separate the fuel and core-box. The relative high values in the transmission response matrices also suggest that the single reflector node of 7.71 cm is too small to represent the total reflector response and thus the definition of the appropriate albedo boundary condition, to represent the response of the rest of the water nodes, is essential.

The next and most important step was to implement the different models into the SAFARI-1 cycle calculation, to show that a practical method for reflector modelling has been established. First a heterogeneous reflector representation was defined to be the reference diffusion solution. This reference model uses the explicit equivalent nodal parameters for all eight identified reflector cuts. By comparison to geometrically reduced models, the homogenisation error (where the core-box and first water node were smeared together) was quantified. The effect on reactivity (40 pcm) and power distribution (maximum 0.72 %) is negligible. Some large homogenisation effects were seen in the corner positions, where the thermal flux differs with up to 10% from the reference model. The main reason for the difference in corner flux values, is that the corner nodes have two core-reflector faces. Since these positions are far from the fuel assemblies, the flux levels are much lower, and therefore the relative differences are also larger. The effect of the geometrically reduced model, where the two outer reflector nodes were replaced by an equivalent NGET albedo boundary condition, was also quantified. In this case, the reactivity effect (37 pcm) and thermal flux changes (maximum 2.2 % outside the active core) are relative small, but the assembly powers differs with up to 1.66 % from the reference model. No corner effects were seen in this case.

Ultimately the combined effect of homogenisation and size reduction is important since it represent the most practical representation of the reflector region. In this case the effects of reflector homogenisation and size reduction are combined. Some of the effects may also cancel out. The core reactivity increased by 78 pcm and the assembly power differences are 1.7 % at BOC (in control rod positions with low relative power) and 0.78 % at EOC. The thermal flux differences in the corners are slightly lower at 7.7 %, showing some cancellation in the effects of homogenisation and model size reduction. The differences seen, is considered to be within acceptable accuracy for day-to-day cycle analysis.

The most important benefit in the use of the reduced model is the reduction in the calculational time by more than 50 %. The iterative behaviour of the reduced model is also much more stable

since less time is spent in trying to solve for the fluxes in the outer reflector far away from the areas of interest. Another very positive result is that the differences reported remain very similar throughout the cycle calculation and thus insensitive to burn-up changes.

In an attempt to improve the simplicity and practical use of the reflector models even further, the sensitivity of the reflector parameters to the environment used to generate it, was tested in the SAFARI-1 cycle calculation. The first attempt to replace all eight of the identified core-reflector environments or cuts with a single set of ENPs from Cut 1 (the simplest model, with only fuel and ex-core reflector) produced reasonable but unexpected results with only 5 pcm differences in reactivity and power differences less than 1.2 % compared to the reference case. The largest differences were seen in the thermal fluxes in the outer reflector assemblies bordering the core-box not facing the pool side. The effects in the corner assemblies are the largest, with up to 12 % differences. This clearly shows that the Cut 1 reflector parameters are not appropriate in any of these core-reflector interface positions except for the row of fuel facing the pool-side.

The next natural step was to select one other cut to represent all of these positions and to see if the results improve. The reduced model with two reflector cuts (Cut 1 and Cut 7, with hollow beryllium between the fuel and reflector) was investigated and compared to the reference case. The results show that the reactivity difference increased to 88 pcm, but the power differences (no more than 1.2 %) and the thermal flux differences (no more than 3.6 %) is much improved and the corner effects all but disappeared (about 1 % differences). This is a very promising result.

It can be concluded that a practical and simplified methodology has been established to calculate multi-group NGET parameters to represent the ex-core reflector regions in the SAFARI-1 reactor. Simplifications, like using fewer 1D reflector models to represent the multiple different environments have proven to be achievable without large penalties in accuracy. The simplified model also allows much shorter execution times and leads to more stable solutions. The study also shows that the selection of the correct environment to represent the reflector is important and this can be further optimised.

7.2 Future work

The methodology and calculational path for establishing a simplified representation of the ex-core reflector regions for SAFARI-1 has been established. The same methodology can be tested on other MTRs, where the reflector assemblies may be different (for example beryllium-oxide or graphite) to assure that the method is still valid. The current tests were also performed with a single cycle whereas ideally multiple cycles and comparisons with plant data and measurements can be included. This falls outside the scope of the current study, but will be performed as part of the SAFARI-1 model validation project in future.

The NGET parameters prove to be accurate in the multi-group application, but sensitivities to the core environment still needs to be taken into account. The NGET-RM (NGET-Response Matrix)

method has shown potential, for PWR and BWR applications, to be less dependent on the environment and should be investigated in future.

The possible refinement of the ex-core reflector models to include details of facilities in the outer water reflector should also be considered. Facilities such as beam lines or large irradiation facilities that may affect the reflector response should be studied.

Previous studies into NGET reflector parameters for PWR and BWR reactors have reported errors due to two-dimensional effects at corners in a reactor core. This may be a limitation to the use of one-dimensional NGET parameters. These 2D effects were however only noticed in the the so-called inner corners, where re-entrant boundaries are found, and are not applicable to the outer corners found in the SAFARI-1 model. Nevertheless future studies should investigate if more advanced models, that may include two-dimensional effects, are required.

Appendix A

Comparison between SCALE and Serpent

This section contains results for the SCALE model validation. The one-dimensional verification model (see Figure 3.3) is run in SCALE and in Serpent, and the 6 group results are compared. Graphs are given for the differences in flux and total cross-sections, per material region, per broad energy group. Tables are given for the differences in scatter cross-sections for these material regions (fuel, core-box and three water nodes).

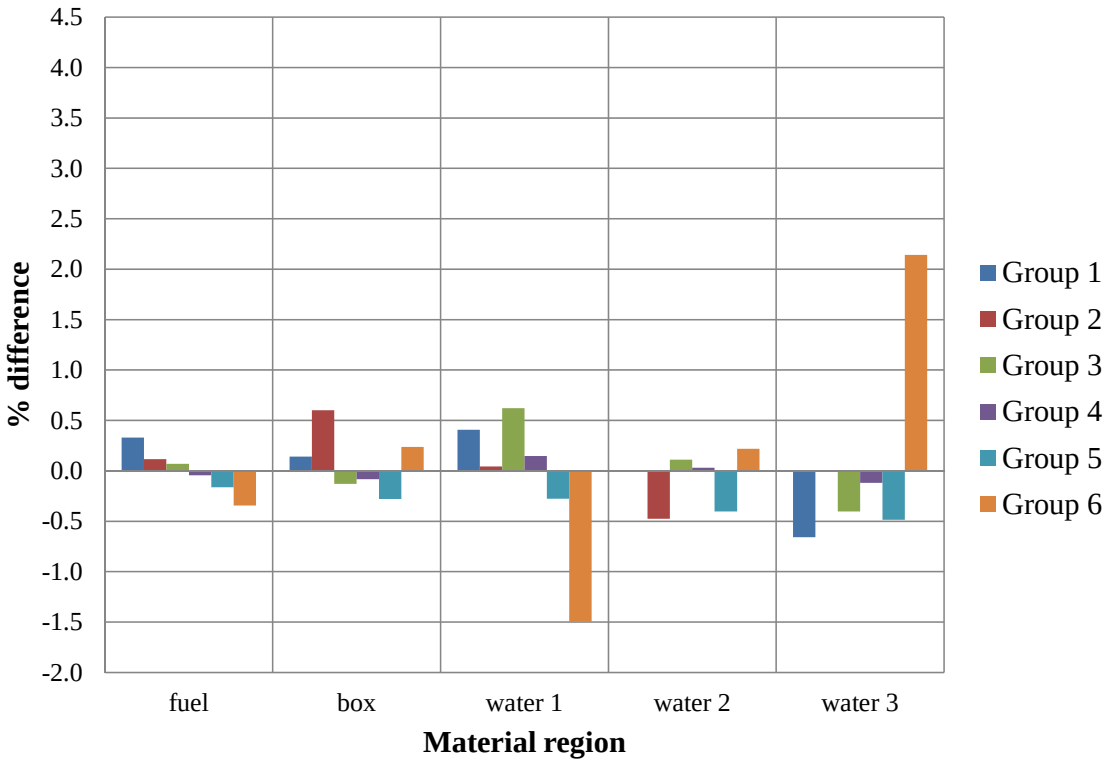

Figure A.1: Percentage differences between in the neutron flux calculated by SCALE and Serpent

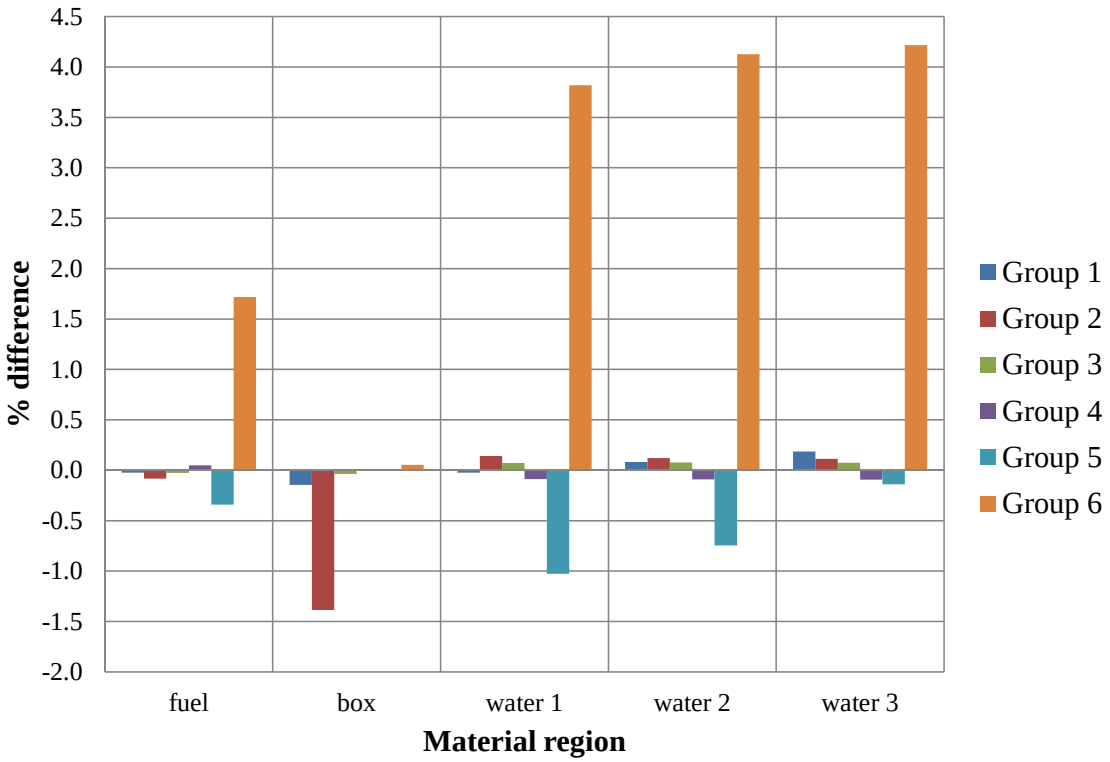

Figure A.2: Percentage differences between in the total cross-sections calculated by SCALE and Serpent

Table A.1: Percentage differences in the scatter matrix calculated by SCALE and Serpent, for the fuel node

From/To	1	2	3	4	5	6
1	-0.045	0.022	0.000	0.000	0.000	0.000
2	0.000	-0.102	0.019	0.000	0.000	0.000
3	0.000	0.000	-0.022	-0.039	-0.007	0.036
4	0.000	0.000	-0.003	-0.261	0.148	0.162
5	0.000	0.000	0.000	0.000	0.075	-0.442
6	0.000	0.000	0.000	0.000	-0.405	1.756

Table A.2: Percentage differences in the scatter matrix calculated by SCALE and Serpent, for the core-box node

From/To	1	2	3	4	5	6
1	-0.136	-0.009	0.000	0.000	0.000	0.000
2	0.000	-1.386	0.000	0.000	0.000	0.000
3	0.000	0.000	-0.033	-0.001	0.000	0.000
4	0.000	0.000	-0.002	0.002	0.002	0.000
5	0.000	0.000	0.000	0.006	0.056	-0.058
6	0.000	0.000	0.000	0.000	0.001	0.024

Table A.3: Percentage differences in the scatter matrix calculated by SCALE and Serpent, for the first water node

From/To	1	2	3	4	5	6
1	-0.032	0.007	0.000	0.000	0.000	0.000
2	0.000	0.068	0.072	0.000	0.000	0.000
3	0.000	0.000	0.060	-0.042	-0.005	0.058
4	0.000	0.000	-0.004	-0.474	0.147	0.243
5	0.000	0.000	0.000	0.013	1.057	-2.088
6	0.000	0.000	0.000	0.000	-0.604	4.385

Table A.4: Percentage differences in the scatter matrix calculated by SCALE and Serpent, for the second water node

From/To	1	2	3	4	5	6
1	0.055	0.028	-0.001	0.000	0.000	0.000
2	0.000	0.028	0.092	0.000	0.000	0.000
3	0.000	0.000	-0.048	0.041	0.016	0.067
4	0.000	0.000	-0.004	-0.472	0.193	0.194
5	0.000	0.000	0.000	0.008	0.578	-1.324
6	0.000	0.000	0.000	0.000	-0.616	4.701

Table A.5: Percentage differences in the scatter matrix calculated by SCALE and Serpent, for the third water node

From/To	1	2	3	4	5	6
1	0.117	0.071	-0.002	0.000	0.000	0.000
2	0.000	0.056	0.056	0.001	0.000	0.000
3	0.000	0.000	-0.047	0.063	-0.009	0.068
4	0.000	0.000	-0.006	-0.571	0.180	0.305
5	0.000	0.000	0.000	-0.004	-0.195	0.062
6	0.000	0.000	0.000	0.000	-0.633	4.808

Appendix B

Albedo results

This section contains results for the 238 group albedo values for the eight 1D reflector cuts (refer to Figure 3.5). Results are also provided for Cut 1 with a burnt fuel driver zone. Albedo values are calculated according with Equation 5.1.

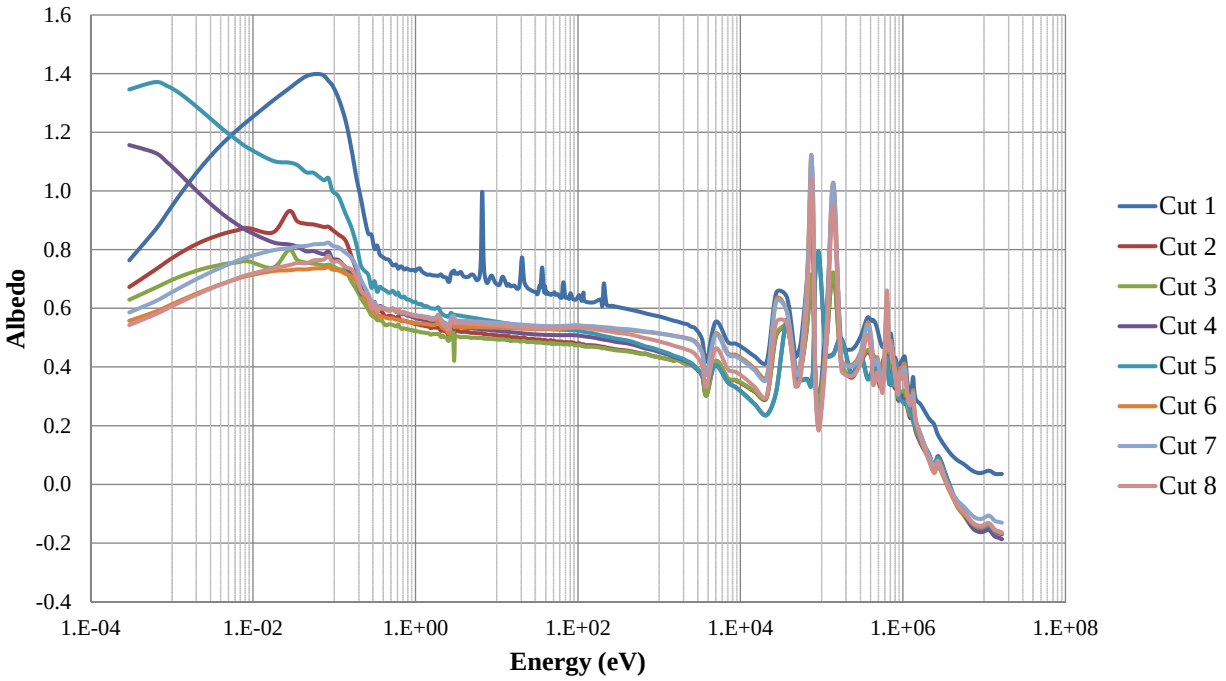

Figure B.1: Albedo at the core-reflector interface for all eight 1D reflector models

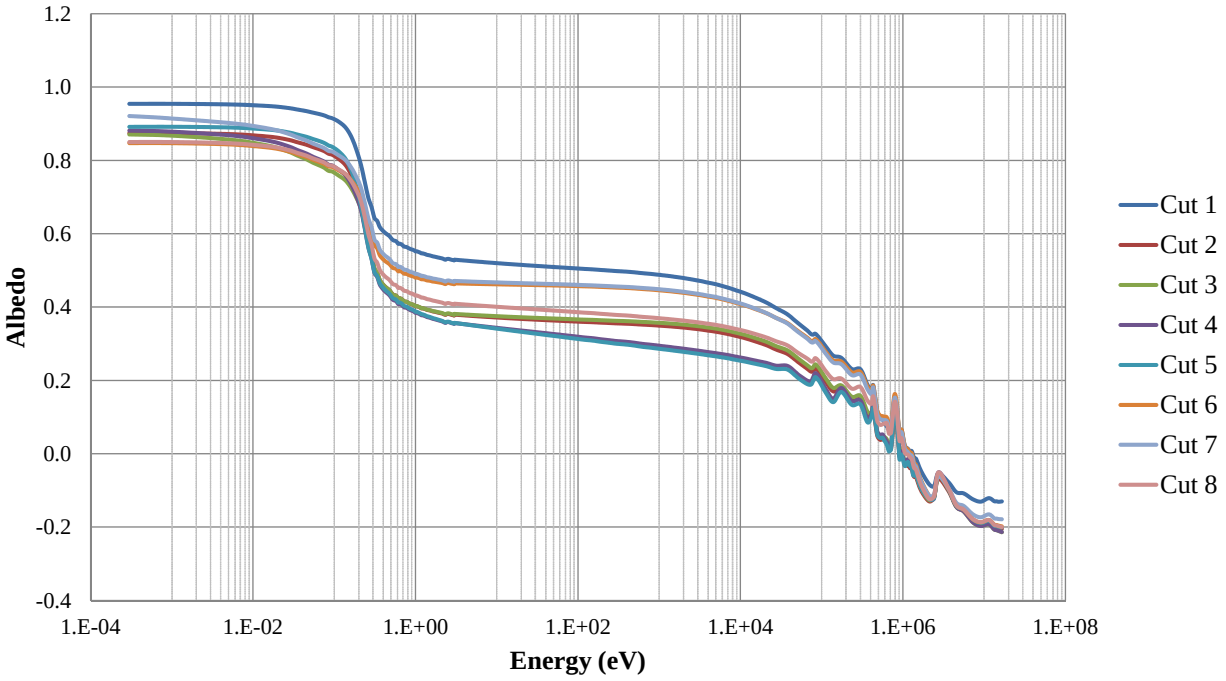

Figure B.2: Albedo after the first water node for all eight 1D reflector models

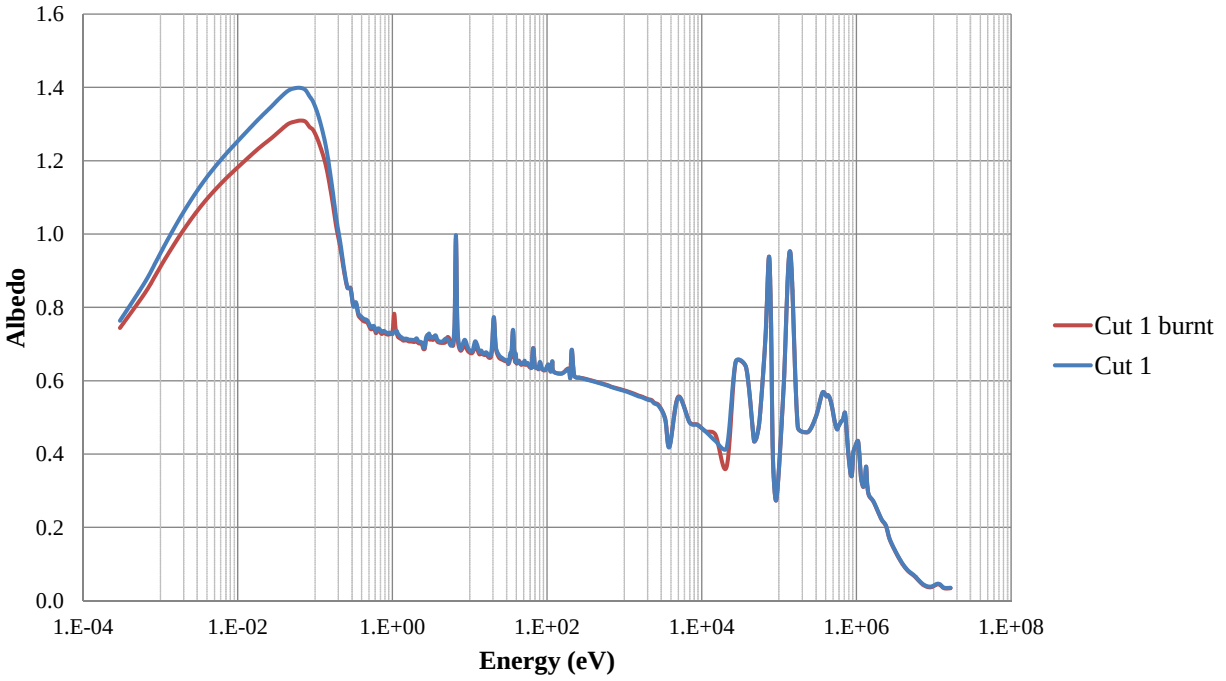

Figure B.3: Albedo at the core-reflector interface for Cut 1 with fresh and burnt fuel driver zone

Appendix C

Response matrix results

This section contains results for the broad-group reflection and transmission response matrices for Cuts 2 - 8 (refer to Figure 3.5), as well as for Cut 1 with a burnt fuel driver zone. In the following tables, the reflection matrices are given on the left hand side, and the transmission matrices are given on the right hand side.

Table C.1: Reflection and transmission matrices for Cut 2

To/From	1	2	3	4	5	6
1	0.09	0.00	0.00	0.00	0.00	0.00
2	0.21	0.13	0.00	0.00	0.00	0.00
3	0.06	0.19	0.03	0.00	0.00	0.00
4	0.01	0.03	0.11	-0.22	0.00	0.00
5	0.01	0.02	0.06	0.17	-0.27	0.03
6	0.02	0.06	0.18	0.42	0.66	0.39

To/From	1	2	3	4	5	6
1	0.33	0.00	0.00	0.00	0.00	0.00
2	0.16	0.29	0.00	0.00	0.00	0.00
3	0.06	0.15	0.28	0.00	0.00	0.00
4	0.01	0.03	0.07	0.09	0.00	0.00
5	0.01	0.02	0.04	0.07	0.06	0.02
6	0.02	0.06	0.16	0.33	0.38	0.36

Table C.2: Reflection and transmission matrices for Cut 3

To/From	1	2	3	4	5	6
1	0.09	0.00	0.00	0.00	0.00	0.00
2	0.20	0.13	0.00	0.00	0.00	0.00
3	0.06	0.19	0.03	0.00	0.00	0.00
4	0.01	0.03	0.11	-0.22	0.00	0.00
5	0.01	0.02	0.05	0.16	-0.29	0.03
6	0.02	0.06	0.18	0.42	0.67	0.37

To/From	1	2	3	4	5	6
1	0.33	0.00	0.00	0.00	0.00	0.00
2	0.16	0.29	0.00	0.00	0.00	0.00
3	0.06	0.14	0.27	0.00	0.00	0.00
4	0.01	0.03	0.07	0.09	0.00	0.00
5	0.01	0.02	0.04	0.07	0.05	0.02
6	0.02	0.06	0.17	0.33	0.39	0.38

Table C.3: Reflection and transmission matrices for Cut 4

To/From	1	2	3	4	5	6
1	0.09	0.00	0.00	0.00	0.00	0.00
2	0.20	0.08	0.00	0.00	0.00	0.00
3	0.06	0.20	0.03	0.00	0.00	0.00
4	0.01	0.03	0.11	-0.22	0.00	0.00
5	0.01	0.02	0.05	0.16	-0.28	0.03
6	0.02	0.07	0.18	0.43	0.66	0.38

To/From	1	2	3	4	5	6
1	0.34	0.00	0.00	0.00	0.00	0.00
2	0.16	0.31	0.00	0.00	0.00	0.00
3	0.06	0.15	0.28	0.00	0.00	0.00
4	0.01	0.03	0.07	0.09	0.00	0.00
5	0.01	0.02	0.04	0.07	0.05	0.02
6	0.02	0.06	0.17	0.33	0.38	0.37

Table C.4: Reflection and transmission matrices for Cut 5

To/From	1	2	3	4	5	6
1	0.09	0.00	0.00	0.00	0.00	0.00
2	0.20	0.07	0.00	0.00	0.00	0.00
3	0.06	0.20	0.04	0.00	0.00	0.00
4	0.01	0.03	0.11	-0.22	0.00	0.00
5	0.01	0.02	0.06	0.17	-0.27	0.03
6	0.02	0.06	0.18	0.43	0.66	0.41

To/From	1	2	3	4	5	6
1	0.33	0.00	0.00	0.00	0.00	0.00
2	0.16	0.31	0.00	0.00	0.00	0.00
3	0.06	0.16	0.28	0.00	0.00	0.00
4	0.01	0.03	0.07	0.08	0.00	0.00
5	0.01	0.02	0.04	0.07	0.05	0.02
6	0.02	0.06	0.16	0.32	0.36	0.33

Table C.5: Reflection and transmission matrices for Cut 6

To/From	1	2	3	4	5	6
1	0.10	0.00	0.00	0.00	0.00	0.00
2	0.19	0.14	0.00	0.00	0.00	0.00
3	0.06	0.19	0.03	0.00	0.00	0.00
4	0.01	0.03	0.11	-0.22	0.00	0.00
5	0.01	0.02	0.05	0.16	-0.30	0.03
6	0.02	0.07	0.19	0.43	0.67	0.37

To/From	1	2	3	4	5	6
1	0.36	0.00	0.00	0.00	0.00	0.00
2	0.15	0.28	0.00	0.00	0.00	0.00
3	0.05	0.14	0.26	0.00	0.00	0.00
4	0.01	0.03	0.07	0.09	0.00	0.00
5	0.01	0.02	0.04	0.06	0.05	0.02
6	0.02	0.06	0.17	0.34	0.39	0.39

Table C.6: Reflection and transmission matrices for Cut 7

To/From	1	2	3	4	5	6
1	0.10	0.00	0.00	0.00	0.00	0.00
2	0.19	0.14	0.00	0.00	0.00	0.00
3	0.06	0.19	0.03	0.00	0.00	0.00
4	0.01	0.03	0.11	-0.22	0.00	0.00
5	0.01	0.02	0.06	0.16	-0.29	0.03
6	0.02	0.06	0.19	0.43	0.67	0.38

To/From	1	2	3	4	5	6
1	0.36	0.00	0.00	0.00	0.00	0.00
2	0.15	0.28	0.00	0.00	0.00	0.00
3	0.05	0.14	0.26	0.00	0.00	0.00
4	0.01	0.03	0.07	0.08	0.00	0.00
5	0.01	0.02	0.04	0.07	0.05	0.02
6	0.02	0.06	0.17	0.33	0.38	0.37

Table C.7: Reflection and transmission matrices for Cut 8

To/From	1	2	3	4	5	6
1	0.10	0.00	0.00	0.00	0.00	0.00
2	0.19	0.12	0.00	0.00	0.00	0.00
3	0.06	0.19	0.03	0.00	0.00	0.00
4	0.01	0.03	0.11	-0.22	0.00	0.00
5	0.01	0.02	0.05	0.16	-0.29	0.03
6	0.02	0.06	0.18	0.43	0.67	0.37

To/From	1	2	3	4	5	6
1	0.35	0.00	0.00	0.00	0.00	0.00
2	0.15	0.29	0.00	0.00	0.00	0.00
3	0.06	0.15	0.27	0.00	0.00	0.00
4	0.01	0.03	0.07	0.09	0.00	0.00
5	0.01	0.02	0.04	0.07	0.05	0.02
6	0.02	0.06	0.17	0.34	0.39	0.39

Table C.8: Reflection and transmission matrices for Cut 1 with a burnt fuel driver zone

To/From	1	2	3	4	5	6
1	0.11	0.00	0.00	0.00	0.00	0.00
2	0.18	0.15	0.00	0.00	0.00	0.00
3	0.06	0.19	0.04	0.00	0.00	0.00
4	0.01	0.03	0.11	-0.23	0.00	0.00
5	0.01	0.02	0.06	0.17	-0.27	0.04
6	0.02	0.07	0.19	0.44	0.68	0.43

To/From	1	2	3	4	5	6
1	0.37	0.00	0.00	0.00	0.00	0.00
2	0.15	0.28	0.00	0.00	0.00	0.00
3	0.05	0.14	0.25	0.00	0.00	0.00
4	0.01	0.03	0.06	0.07	0.00	0.00
5	0.01	0.02	0.04	0.06	0.05	0.02
6	0.02	0.06	0.17	0.32	0.34	0.30

Appendix D

SAFARI-1 results, using eight reflector models

This section contains comparisons between various calculational models for SAFARI-1, as discussed in Chapter 6. All models discussed in this section, uses the eight 1D models (see Figure 3.5) for reflector modelling.

D.1 Effects of homogenisation

In Tables D.1 and D.2 the effect of homogenisation is investigated. For this study, the reference model is compared to the same model, but with the core-box and first water node represented as a homogenised reflector node. The whole reflector is still modelled (i.e. no size reduction).

Table D.1: Effect of homogenisation on the core model: cycle comparison

Time (days)	k-eff Reference	k-eff Homogenised	Difference (pcm)
0.00	0.99998	1.00046	48
0.09	0.99968	1.00063	95
0.12	0.99938	0.99966	28
0.95	0.99999	1.00023	24
3.95	1.00036	1.00074	38
6.95	0.99982	1.00013	31
9.53	1.00000	1.00027	27
9.53	0.99964	1.00030	66
12.53	1.00045	1.00083	38
15.54	0.99993	1.00030	37
18.54	0.99997	1.00046	49
21.54	1.00032	1.00060	28
24.54	0.99973	1.00009	36
27.54	0.99969	0.99993	24
29.71	1.00020	1.00056	36

Table D.2: Effect of homogenisation on the core model: leakage summary

Difference in leakage (%)	BOC	EOC
Total	-0.12	-0.07
Axial	-0.25	-0.13
Radial	-0.06	-0.04
Radial epi-thermal	-0.13	-0.13
Radial thermal	-0.74	-0.89

D.2 Effects of size reduction

In Tables D.3 to D.8, the effect of size reduction is investigated. For this study, the homogenised, full reflector model is compared to the homogenised but reduced reflector model. Therefore, only the impact of size reduction is observed. In the reduced model, the part of the reflector that has been left out, is replaced by NGET albedo boundary conditions.

Table D.3: Effect of size reduction on the core model: cycle comparison

Time (days)	k-eff Homogenised	k-eff Reduced	Difference (pcm)
0.00	1.00046	1.00088	42
0.09	1.00063	1.00106	43
0.12	0.99966	1.00009	43
0.95	1.00023	1.00062	39
3.95	1.00074	1.00113	39
6.95	1.00013	1.00052	39
9.53	1.00027	1.00066	39
9.53	1.00030	1.00068	38
12.53	1.00083	1.00121	38
15.54	1.00030	1.00067	37
18.54	1.00046	1.00082	36
21.54	1.00060	1.00095	35
24.54	1.00009	1.00044	35
27.54	0.99993	1.00026	33
29.71	1.00056	1.00088	32

Table D.4: Effect of size reduction on the core model: leakage summary

Difference in leakage (%)	BOC	EOC
Total	-0.25	-0.09
Axial	-0.22	0.01
Radial	-0.26	-0.12
Radial epi-thermal	-0.21	-0.06
Radial thermal	0.25	0.50

Table D.5: Effect of size reduction on the core model: power at BOC

I/J	1	2	3	4	5	6	7	8	9
A									
B			-0.30	-0.33	-0.54		-0.55		
C				-0.25	0.82	-0.26	0.83	0.00	
D			-0.48	-0.26	-0.30		-0.27		
E				-0.27	0.97	-0.29	1.30	0.00	
F			-0.27	-0.29	-0.30		0.00		
G				0.00	1.66	0.00	0.92	0.00	
H			-0.34	0.00	0.00	0.37	0.00		

Table D.6: Effect of size reduction on the core model: power at EOC

I/J	1	2	3	4	5	6	7	8	9
A									
B			0.00	-0.36	0.00		-0.27		
C				-0.27	-0.36	0.00	0.00	0.00	
D			-0.28	0.00	0.00		-0.26		
E				0.00	0.00	0.00	0.00	0.32	
F			0.00	0.00	0.00		0.00		
G				0.00	0.00	0.31	0.00	0.34	
H			0.00	0.39	0.36	0.37	0.00		

Table D.7: Effect of size reduction on the core model: thermal flux at BOC

I/J	1	2	3	4	5	6	7	8	9
A	1.98	0.48	0.05	0.53	0.02	0.00	0.05	0.04	0.01
B	1.31	0.42	0.49	0.74	0.75	0.58	0.88	0.49	0.13
C	0.92	0.30	0.36	0.73	0.53	1.06	0.71	1.04	0.46
D	0.68	0.27	0.51	0.80	0.92	0.99	1.27	1.03	1.10
E	0.36	0.16	0.38	0.77	0.67	1.16	0.92	1.47	1.93
F	0.16	0.15	0.55	0.88	1.05	1.10	1.39	1.24	1.76
G	0.04	0.10	0.50	0.99	0.83	1.32	1.00	1.45	1.72
H	-0.36	-0.13	0.84	1.36	1.57	1.75	1.55	0.97	1.78

Table D.8: Effect of size reduction on the core model: thermal flux at EOC

I/J	1	2	3	4	5	6	7	8	9
A	2.20	0.65	0.17	0.49	0.07	0.01	0.04	0.05	0.05
B	1.52	0.59	0.57	0.64	0.53	0.38	0.55	0.33	0.10
C	1.13	0.46	0.44	0.59	0.41	0.60	0.49	0.66	0.36
D	0.88	0.42	0.55	0.62	0.55	0.55	0.71	0.67	0.96
E	0.55	0.32	0.45	0.61	0.46	0.66	0.61	0.98	1.74
F	0.36	0.30	0.60	0.71	0.67	0.66	0.82	0.85	1.60
G	0.23	0.25	0.58	0.85	0.64	0.87	0.75	0.99	1.58
H	-0.16	0.04	0.92	1.29	1.31	1.36	1.13	0.73	1.73

D.3 Accumulative effects of homogenisation and size reduction

In Tables D.9 and D.10 the effects of homogenisation and size reduction together are investigated. For this study, the reference calculation is compared to the reduced reflector model (for which the reflector region is homogenised).

Table D.9: Effect of homogenisation and size reduction on the core model: cycle comparison

Time (days)	k-eff Reference	k-eff Reduced	Difference (pcm)
0.00	0.99998	1.00088	90
0.09	0.99968	1.00106	138
0.12	0.99938	1.00009	71
0.95	0.99999	1.00062	63
3.95	1.00036	1.00113	77
6.95	0.99982	1.00052	70
9.53	1.00000	1.00066	66
9.53	0.99964	1.00068	104
12.53	1.00045	1.00121	76
15.54	0.99993	1.00067	74
18.54	0.99997	1.00082	85
21.54	1.00032	1.00095	63
24.54	0.99973	1.00044	71
27.54	0.99969	1.00026	57
29.71	1.00020	1.00088	68

Table D.10: Effect of homogenisation and size reduction on the core model: leakage summary

Difference in leakage (%)	BOC	EOC
Total	-0.37	-0.15
Axial	-0.47	-0.12
Radial	-0.33	-0.16
Radial epi-thermal	-0.34	-0.19
Radial thermal	-0.49	-0.40

D.4 Sensitivity to burnup in the fuel driver zone

The last investigation using all eight 1D reflector models, is to test whether the reflector is sensitive to the fuel burnup. In Tables D.11 and D.12, the reduced model is compared to another reduced model, where the reflector cross-sections were prepared for a fuel driver zone that has been burnt 40 % for U-235.

Table D.11: Effect of burnup in fuel driver zone: cycle comparison

Time (days)	k-eff Reduced	k-eff Burnt fuel	Difference (pcm)
0.00	1.00088	1.00100	12
0.09	1.00106	1.00117	11
0.12	1.00009	1.00021	12
0.95	1.00062	1.00073	11
3.95	1.00113	1.00124	11
6.95	1.00052	1.00064	12
9.53	1.00066	1.00078	12
9.53	1.00068	1.00080	12
12.53	1.00121	1.00133	12
15.54	1.00067	1.00079	12
18.54	1.00082	1.00095	13
21.54	1.00095	1.00108	13
24.54	1.00044	1.00056	12
27.54	1.00026	1.00039	13
29.71	1.00088	1.00102	14

Table D.12: Effect of burnup in fuel driver zone: leakage summary

Difference in leakage (%)	BOC	EOC
Total	-0.01	-0.02
Axial	-0.01	-0.01
Radial	-0.01	-0.02
Radial epi-thermal	0.08	0.07
Radial thermal	0.89	0.85

Appendix E

SAFARI-1 results, using one or two reflector models

This section contains comparisons between various calculational models for SAFARI-1. The models discussed in this section, do not use all eight 1D models (see Figure 3.5) for reflector modelling. Only Cuts 1 and 7 are used.

E.1 Explicit model with one reflector cut

Table E.1: Effect of using one explicit reflector model for all reflector nodes: cycle comparison

Time (days)	k-eff Reference	k-eff 1 cut explicit	Difference (pcm)
0.00	0.99998	1.00194	196
0.09	0.99968	1.00211	243
0.12	0.99938	1.00114	176
0.95	0.99999	1.00170	171
3.95	1.00036	1.00222	186
6.95	0.99982	1.00164	182
9.53	1.00000	1.00182	182
9.53	0.99964	1.00184	220
12.53	1.00045	1.00241	195
15.54	0.99993	1.00190	197
18.54	0.99997	1.00208	211
21.54	1.00032	1.00224	192
24.54	0.99973	1.00176	203
27.54	0.99969	1.00163	194
29.71	1.00020	1.00227	206

Table E.2: Effect of using one explicit reflector model for all reflector nodes: leakage summary

Difference in leakage (%)	BOC	EOC
Total	-0.47	-0.48
Axial	-0.01	0.06
Radial	-0.65	-0.69
Radial epi-thermal	-0.08	-0.10
Radial thermal	5.17	5.26

E.2 Reduced model with one reflector cut

Tables E.3 and E.4 show comparisons for the cycle evolution and core leakage for the reduced model using only Cut 1 to represent the reflector, compared to the reference model.

Table E.3: Effect of using one reduced reflector model for all reflector nodes: cycle comparison

Time (days)	k-eff Reference	k-eff 1 cut reduced	Difference (pcm)
0.00	0.99998	1.00010	12
0.09	0.99968	1.00028	60
0.12	0.99938	0.99931	-7
0.95	0.99999	0.99988	-11
3.95	1.00036	1.00038	2
6.95	0.99982	0.99976	-6
9.53	1.00000	0.99991	-9
9.53	0.99964	0.99994	30
12.53	1.00045	1.00048	3
15.54	0.99993	0.99994	1
18.54	0.99997	1.00011	14
21.54	1.00032	1.00024	-8
24.54	0.99973	0.99975	2
27.54	0.99969	0.99959	-10
29.71	1.00020	1.00022	2

Table E.4: Effect of using one reduced reflector model for all reflector nodes: leakage summary

Difference in leakage (%)	BOC	EOC
Total	-0.03	0.00
Axial	-0.10	-0.03
Radial	-0.01	0.02
Radial epi-thermal	-0.49	-0.49
Radial thermal	-4.83	-5.06

E.3 Explicit model with two reflector cuts

Tables E.5 and E.6 show comparisons for the cycle evolution and core leakage for the explicit model using two cuts to represent the reflector, compared to the reference model.

Table E.5: Effect of using two explicit reflector models for all reflector nodes: cycle comparison

Time (days)	k-eff Reference	k-eff 2 cuts explicit	Difference (pcm)
0.00	0.99998	1.00007	9
0.09	0.99968	1.00025	57
0.12	0.99938	0.99928	-10
0.95	0.99999	0.99983	-16
3.95	1.00036	1.00033	-3
6.95	0.99982	0.99973	-9
9.53	1.00000	0.99988	-12
9.53	0.99964	0.99991	27
12.53	1.00045	1.00046	1
15.54	0.99993	0.99993	0
18.54	0.99997	1.00009	12
21.54	1.00032	1.00024	-8
24.54	0.99973	0.99975	2
27.54	0.99969	0.99960	-9
29.71	1.00020	1.00024	4

Table E.6: Effect of using two explicit reflector models for all reflector nodes: leakage summary

Difference in leakage (%)	BOC	EOC
Total	-0.02	0.01
Axial	-0.04	0.01
Radial	-0.02	0.01
Radial epi-thermal	0.01	0.03
Radial thermal	0.20	0.20

E.4 Reduced model with two reflector cuts

Tables E.7 and E.8 show comparisons for the cycle evolution and core leakage for the reduced model using two cuts to represent the reflector, compared to the reference model.

Table E.7: Effect of using two reduced reflector models for all reflector nodes: cycle comparison

Time (days)	k-eff Reference	k-eff 2 cuts reduced	Difference (pcm)
0.00	0.99998	1.00089	91
0.09	0.99968	1.00107	139
0.12	0.99938	1.00010	72
0.95	0.99999	1.00067	68
3.95	1.00036	1.00119	83
6.95	0.99982	1.00058	76
9.53	1.00000	1.00075	75
9.53	0.99964	1.00077	113
12.53	1.00045	1.00133	88
15.54	0.99993	1.00080	87
18.54	0.99997	1.00097	100
21.54	1.00032	1.00112	80
24.54	0.99973	1.00063	90
27.54	0.99969	1.00048	79
29.71	1.00020	1.00112	92

Table E.8: Effect of using two reduced reflector models for all reflector nodes: leakage summary

Difference in leakage (%)	BOC	EOC
Total	-0.18	-0.18
Axial	-0.15	-0.09
Radial	-0.19	-0.22
Radial epi-thermal	0.00	-0.02
Radial thermal	1.72	1.74

Bibliography

[1] A. Hébert. *Applied reactor physics*. Presses inter Polytechnique, 2009.

[2] K. Koebke. A new approach to homogenization and group condensation. Technical report, IAEA Technical Committee Meeting on Homogenization Methods in Reactor Physics, November 1978.

[3] K. Koebke. Advances in homogenization and dehomogenization. *Proceedings of ANS/ENS International Topical Meeting on Advances in Mathematical Methods for the Solution of Nuclear Engineering Problems*, 2:59–73, April 1981.

[4] K.S. Smith. *Spatial homogenization methods for light water reactor analysis*. PhD thesis, Massachusetts Institute of Technology, June 1980.

[5] K.S. Smith. Assembly homogenization techniques for light water reactor analysis. *Progress in Nuclear Energy*, 17(3):303–335, 1986.

[6] E.Z. Müller. *Development of an environment-insensitive PWR radial reflector model applicable to modern nodal reactor analysis methods*. PhD thesis, Potchefstroom University for CHE, Faculty of Natural Sciences, 1989.

[7] F. Reitsma. The application of advanced homogenization models to the reflector regions of boiling water reactors. Master's thesis, Potchefstroom University for CHE, Faculty of Natural Sciences, 1998.

[8] R.H. Prinsloo, L.E. Moloko, P.M. Bokov, G. Stander, K. Elsakhawy, and S.A. Theron. SAFARI-1 benchmark specification. Internal Report RRT-SAFARI-08-22, South African Nuclear Energy Corporation, 2008.

[9] W.R. Joubert, F. Reitsma, and D.I. Tomašević. Comparative study of nodal cross section models applied to MTR core analysis. In *PHYSOR 2002, New Frontiers of Nuclear Technology: Reactor Physics, Safety an High-Performance Computing*. Seoul, Korea, October 2002.

[10] M.M.R. Williams. *Mathematical methods in particle transport theory*. Butterworths, London, 1971.

[11] J.J. Duderstadt and L.J. Hamilton. *Nuclear reactor analysis*. John Wiley and Sons, Inc., New York, 1976.

[12] R.J.J. Stamm'ler and M.J. Abbate. *Methods of steady-state reactor physics in nuclear design*. Academic Press London, 1983.

[13] S.Ö. Lindahl and Z. Weiss. The response matrix method. *Advances in Nuclear Science and Technology*, 13:73–154, 1981.

[14] W.M. Stacey. *Nuclear reactor physics*. John Wiley and Sons, Inc., New York, 2007.

[15] D.G. Cacuci et al. *Handbook of Nuclear Engineering*. Springer, 2010.

[16] R.D. Lawrence. Progress in nodal methods for the solution of the neutron diffusion and transport equations. *Progress in Nuclear Energy*, 17(3):271–301, 1986.

[17] M.R. Wagner. Current trends in multidimensional static reactor calculations. Technical report, Kraftwerk Union AG, Erlangen, Ger.; Du Pont de Nemours (EI) and Co., Aiken, SC (USA). Savannah River Lab.; Energy Research and Development Administration, Aiken, SC (USA). Savannah River Operations Office, 1975.

[18] H. Finnemann, F. Bennewitz, and M.R. Wagner. Interface current techniques for multidimensional reactor calculations. *Atomkernenergie*, 30(2):123–128, 1977.

[19] K.S. Smith. An analytic nodal method for solving the two-group, multidimensional, static and transient neutron diffusion equations. Master's thesis, Massachusetts Institute of Technology, March 1979.

[20] R.D. Lawrence and J. Dorning. A nodal Green's function method for multi-dimensional neutron diffusion calculations. *Nuclear Science and Engineering*, 76:218–231, 1980.

[21] A. Dall'Osso. A spatial rehomogenization method in nodal calculations. *Annals of Nuclear Energy*, 33:869–877, 2006.

[22] F. Reitsma and E.Z. Müller. Evaluation of the use of nodal methods for MTR neutronic analysis. In *17th International Meeting on Reduced Enrichment for Research Reactors (RERTR)*. Williamsburg, Virginia, USA, September 1994.

[23] D.S. Selengut. Diffusion coefficents for heterogeneous systems. *Transactions of the Amercan Nuclear Society*, 3:398, 1960.

[24] P.C. Kalambokas and A.F. Henry. The representation of Light-Water Reflectors by boundary conditions. *Nuclear Science and Engineering*, 61:181–195, 1976.

[25] D.K. Parsons. *The replacement of reflectors and baffles in nodal calculations by albedo boundary conditions*. PhD thesis, Massachusetts Institute of Technology, Department of Nuclear Engineering, 1984.

[26] K. Koebke, H. Haase, L. Hetzelt, and H.J. Winter. Application and verification of the simplified equivalence theory for burnup states. *Nuclear Science and Engineering*, 92(1):56, 1986.

[27] A. Trkov and M. Ravnik. Effective diffusion homogenization of cross sections for Pressurized Water Reactor core calculations. *Nuclear Science and Engineering*, 116:86–95, 1994.

[28] L. Hetzelt and H.J. Winter. Generalization of the equivalent reflector model for the Siemens Standard Core Design Procedure. In *Mathematics and Computation, Reactor Physics and Environmental Analysis in Nuclear Applications*. Madrid, Spain, September 1999.

[29] C. Sandrin, R. Sanchez, and F. Dolce. An analysis of reflector homogenization techniques for full core diffusion calculations. *Nuclear Science and Engineering*, 168:59–72, 2011.

[30] R. Sanchez. Assembly homogenization techniques for core calculations. *Progress in Nuclear Energy*, 51:14–31, 2009.

[31] S.P. Palmtag. *Advanced nodal methods for MOX fuel analysis*. PhD thesis, Massachusetts Institute of Technology, 1997.

[32] K. Koebke, L. Hetzelt, M.R. Wagner, and H.L. Winter. Principles and application of advanced nodal reactor analysis methods. *Atomkernenergie*, 46:224, 1985.

[33] E.Z. Müller. The one-dimensional normalised generalised equivalence theory (NGET) for generating equivalent diffusion theory group constants for PWR reflector regions. Technical Report PEL 303, Atomic Energy Corporation of South Africa, January 1991.

[34] C.V. Parks and US Nuclear Regulatory Commission. *SCALE: A modular code system for performing standardized computer analyses for licensing evaluation*. Oak Ridge National Laboratory, Oak Ridge, TN, version 6 edition, 2009. Available from Radiation Safety Information Computational Centre at Oak Ridge National Laboratory as CCC-750.

[35] M.D. DeHart. NEWT: a new transport algorithm for two-dimensional discrete ordinates analysis in non-orthogonal geometries. *ORNL/TM-2005/39*, 6, 2006.

[36] E.Z. Müller. EQUIVA-1: A code for generating one-dimensional NGET cross sections for PWR ex-core regions. Technical Report PEL 301, Atomic Energy Corporation of South Africa, January 1991.

[37] E.Z. Müller. EQUIVA-2: A code for generating environment-insensitive equivalent nodal parameters for PWR reflector regions. Technical Report PEL 307, Atomic Energy Corporation of South Africa, March 1991.

[38] R.H. Prinsloo. OSCAR-4 system overview. Technical report, South African Nuclear Energy Corporation, January 2012.

[39] G. Stander, R.H. Prinsloo, E.Z. Müller, and D.I. Tomašević. OSCAR-4 code system application to the SAFARI-1 reactor. In *PHYSOR 2008, International Conference on Reactor Physics, Nuclear Power: A Sustainable Resource*, Interlaken, Switzerland, September 2008.

[40] W.R. Joubert and Z.J. Weiss. A nodal solution of the interface current equations. In *Topical meeting on Advances in Reactor Physics*, Charleston, USA, August 1992.

[41] D.L. Vogel and Z.J. Weiss. A general, multigroup formulation of the analytic nodal method. In *International Topical Meeting on Advances in Reactor Physics*, Charleston, South Carolina, USA, March 1992.

[42] E.Z. Müller. Validation of the one-dimensional NGET homogenised baffle/reflector model. Technical Report RTE01-2/2-031, Atomic Energy Corporation of South Africa, December 1987.

[43] M.D. DeHart and S.M. Bowman. Reactor physics methods and analysis capabilities in SCALE. *Nuclear Technology*, 174:196–213, May 2011.

[44] J. Leppänen. PSG2 / Serpent - a continuous-energy monte carlo reactor physics burnup calculation code. Technical report, VVT Technical Research Centre of Finland, March 2012.

[45] E.Z. Müller. Environment-insensitive equivalent diffusion theory group constants for pressurized water reactor radial reflector regions. *Nuclear Science and Engineering*, 103:359 – 376, 1989.

[46] F. Reitsma and E.Z. Müller. Flexible exposure and nodal mesh treatment in the 3D nodal simulator mgrac: application to a MTR case with axially movable assemblies. In *PHYSOR 2002, New Frontiers of Nuclear Technology: Reactor Physics, Safety an High-Performance Computing*. Seoul, Korea, October 2002.

[47] E. Villarino and D. Hergenreder. Calculation of the core parameters measured during the commisioning of the OPAL reactor. In *PHYSOR 2010, Advances in Reactor Physics to Power the Nuclear Renaissance*. Pittsburgh, Pennsylvania, USA, May 2010.

[48] S.E. Day, M.P. Butler, and W.J. Garland. Calculations in support of the MNR core conversion. In *International Meeting on Reduced Enrichment for Research and Test Reactors*. Bariloche, Argentina, November 2002.

[49] A.M. Hassanain, N.M.A. Mohamed, N.M. Aly, A.A. Badawi, and M.A. Gaheen. Neutron flux characterization fo radioisotope production at ETRR-2. *World Academy of Science, Engineering and Technology*, 49:619–623, 2011.

[50] S.A. Theron and F. Reitsma. Reflector modelling of small high leakage cores making use of multi-group nodal equivalence theory. In *PHYSOR 2012, Advances in Reactor Physics: Linking Research, Industry, and Education*. Knoxville, Tennessee, USA, April 2012.

[51] S.A. Theron and F. Reitsma. MTR reflector modelling making use of reflector equivalence theory. In *SAIP 2011, the 56th Annual Conference of the South African Institute of Physics*. CSIR Convention Centre, Gauteng, South Africa, July 2011.